Research Article

Targeting Alzheimer's disease hallmarks with the Nrf2 activator Isoeugenol

Ana Silva[1], Sónia Silva[2], Jéssica Macedo[2], Patrícia Moreira[1], Diana Baptista[2], Joana Bicker[2], Ana Fortuna[2], Joana Liberal[3], Beatriz Rodrigues[2], Rosa Resende[1], Armanda E. Santos[1], Cláudia Pereira[1], Maria Teresa Cruz[1]

1. Center for Neuroscience and Cell Biology and Institute for Biomedical Imaging and Life Sciences, Universidade de Coimbra, Portugal; 2. Faculty of Pharmacy, Universidade de Coimbra, Portugal; 3. Universidade de Coimbra, Portugal

Alzheimer´s disease is a neurodegenerative disease and the most common cause of dementia with no cure or treatment. Therefore, the investigation to find a disease-modifying therapeutic is crucial. From a pathophysiological point of view, AD is characterized by the loss of homeostatic functions that control redox and energy metabolism, neuroinflammation, and proteostasis. The transcription factor nuclear factor erythroid 2–related factor 2 (Nrf2) is a master controller of these functions and, in the past decades, recent reports have shown that its overall activity is compromised in AD. Thus, Nrf2 has been considered an attractive molecular target for AD therapeutic research. Most pharmacological Nrf2 activators are small electrophilic molecules that react with cysteine residues present in Kelch-like ECH-Associating protein 1 (Keap1), thereby inducing Nrf2 release and further nuclear translocation and activation. Accordingly, low molecular weight skin allergens, such as dimethyl fumarate, currently used to treat the relapsing forms of multiple sclerosis and with positive results in preventing spatial memory impairments and hippocampal neurodegeneration in rats, are able to activate Nrf2. This activation is well explained by their direct reactivity towards key cysteine residues of Keap1, leading to its dissociation from Nrf2, which in turn is translocated to the nucleus inducing the transcription of over 250 protective genes. Hence, we conducted a ground-breaking study where the potential of Isoeugenol, a skin allergen with electrophilic properties, to activate Nrf2 and revert some AD hallmarks, was investigated. This work was conducted in vitro (in mice microglia cells exposed to LPS and neuronal cells overexpressing the human APP with Swedish mutation, N2a-APPswe) and in vivo (in the AD double transgenic mice, APP/PS1, intranasally administered with Isoeugenol), at an early (6-month-old animals) and late (11-month-old animals) AD stage.

Overall, the results showed that Isoeugenol exhibit a good pharmacokinetic and pharmacodynamic profile. Isoeugenol activates Nrf2 and displays antioxidant and anti-inflammatory effects and reduced the levels of Aβ peptides in in vitro and in vivo models of AD. In addition, its positive effect on metabolism was also demonstrated in vivo, as it reduced the triglyceride and LDL cholesterol levels in treated AD mice. Importantly, Isoeugenol improved the memory deficits observed in APP/PS1 mice, which was more evident in older animals (11-month-old), reinforcing its potential in ameliorating AD hallmarks, even at a late stage.

Ana Silva and Sónia Silva contributed equally to this work. Cláudia Pereira and Maria Teresa Cruz contributed equally as senior authors.

Corresponding authors: Ana Silva, anacrs@cnc.uc.pt; Sónia Silva, sonias@ci.uc.pt

Graphical Abstract
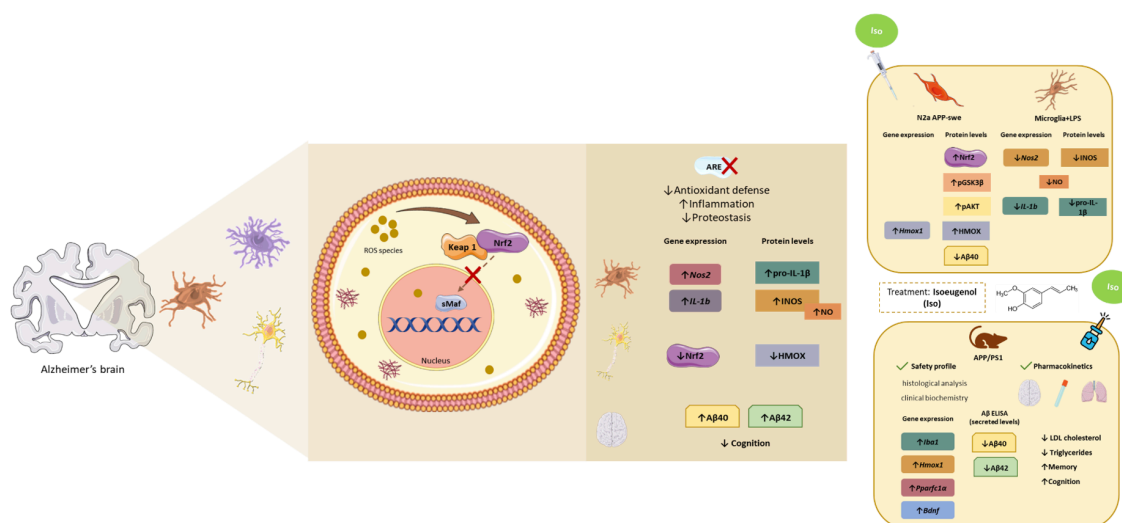
Highlights

- Isoeugenol decreases neuroinflammation in vitro
- Isoeugenol promotes in vitro and in vivo Nrf2 activation
- Isoeugenol decreases in vitro and in vivo Aβ peptides
- Isoeugenol ameliorates memory impairment of APP/PS1 mice

- Intranasal administration of Isoeugenol is safe

1. Introduction

Alzheimer's disease (AD) is one the most common neurodegenerative diseases and the most frequent cause of dementia, accounting for 60% to 70% of the 50 million cases worldwide (Alzheimer's Association, 2020). The slowly progressive neurodegeneration affects the area of the cortex, responsible for the transmission of information and movements, and the hippocampus with relevant functions in long-term memory (Calsolaro and Edison, 2016; Cheignon et al, 2018). AD has implications in the quality of life of patients and their caregivers and imposes an enormous socioeconomic burden (Lane et al, 2018; Tarawneh and Holtzman, 2012). For more than a decade that AD has been considered as a public health priority by the World Health Organization (WHO, 2012, 2017) and in 2019 it was ranked as the sixth leading cause of death (Heron, 2021).

AD can occur early in life (<65 years), thus defined as familial or early-onset AD (EOAD). EOAD is mainly caused by genetic alterations, involving pathogenic mutations in the amyloid-β precursor protein (*APP*) and in the presenilin -1 (*PSEN1*) and -2 (*PSEN2*) genes (Masters et al, 2015; Wang et al, 2017). When occurring after 65 years-old, AD is classified as sporadic or late-onset AD (LOAD), and accounts for about 95% of the cases. LOAD-associated risks include a combination of multiple factors including aging, history of disease, in particular chronic metabolic diseases, and genetics through the presence of allele 4 of the apolipoprotein E gene (*APOE*) (Wang et al, 2017; Breijyeh and Karaman, 2020).

AD neuropathologic hallmarks include Aβ peptides accumulation and consequent amyloid plaques formation, in the extracellular space near neurons, and the presence of intracellular neurofibrillary tangles (NFTs), due to the accumulation of hyperphosphorylated tau protein (Taylor et al, 2002; Serrano-Pozo et al, 2011; Calsolaro and Edison, 2016; Lane et al, 2018; Breijyeh and Karaman, 2020). As a consequence of the neurodegeneration process and synaptic dysfunction, neuroinflammation with activation of microglial cells and oxidative stress occurs (Tönnies and Trushina, 2017; van Eldik et al, 2016; Cheignon et al, 2018).

Although the etiology of this disease is not completely known, an association between the increased incidence of cases with aging is well-known; therefore, early detection is a crucial step for the prevention and treatment of AD (Chen et al, 2016; Alzheimer's Association, 2016). So far, many advances have been made in order to better understand the neuropathology of AD, but there are still no disease-modifying-treatments, with capacity to prevent or cure it (Alzheimer's Association, 2020). The amyloid cascade hypothesis, with exacerbated production of Aβ peptides, which cause cell toxicity and neuronal death, is considered the main hypothesis underlying AD occurrence and has been intensively studied to combat the still existing therapeutic lack (Zuroff et al, 2017; Dong et al, 2019). In fact, there are only four therapeutic drugs for AD treatment: three acetylcholinesterase inhibitors and one non-competitive NMDA receptor antagonist, which only relieves the symptoms associated with memory loss or behavior (Geerts and Grossberg, 2006; Schneider, 2013). Recently, the United States Federal Agency Food and Drug Administration (FDA) approved two antibodies designed to clear Aβ from the brain and block the formation of amyloid plaques (Song et al, 2022), although EMA did not approve it due to unproven safety and clinical benefit.

Importantly, in the past few years, recent reports have shown that the Kelch-like ECH-Associating protein 1 (Keap1)-nuclear factor erythroid 2 related factor 2 (Nrf2)-antioxidant response element (ARE) (Keap1–Nrf2–ARE) signaling pathway is compromised in the context of AD (Bahn and Jo, 2019), thus providing an attractive molecular target for AD therapeutic research (Bellezza et al, 2018; Silva et al, 2020). Nrf2 is a basic leucine zipper transcription factor (bZIP) and one of the most important regulators of the defense mechanisms against oxidative and electrophilic stress in the cell (Battino et al, 2018). The activity of Nrf2 is tightly regulated by two main mechanisms that control Nrf2 protein stability in the cytoplasm. Under physiological conditions, Nrf2 binds to Keap1, a ubiquitin E3 ligase adapter, comprising several redox- and electrophilic-sensitive residues of cysteine, which presents Nrf2 to a Cullin3/Rbx1-dependent E3 ubiquitin ligase complex, that promotes Nrf2 ubiquitination and further degradation in the proteasome. The other mechanism involves Nrf2 phosphorylation in specific serine residues by GSK-3β, leading to degradation domains recognized by β–Transducin Repeat Containing E3 Ubiquitin Protein Ligase (β–TrCP, also an E3 ligase adapter), which signals Nrf2 for ubiquitination mediated by the Cullin-1/Rbx1 complex, resulting in its proteasomal degradation. GSK-3β might be inhibited when phosphorylated at Ser[9] by Ser/Thr protein kinases such as AKT. Hence, it has been suggested that activation of AKT and consequent inactivation of GSK-3β might up-regulate Nrf2 (Cuadrado, 2016; Cuadrado 2018).

Increased reactive oxygen species (ROS) levels or the presence of electrophiles (either endogenous or exogenous) are able to activate Nrf2 through covalent modification of cysteine residues present in Keap1 protein, which become unable to present Nrf2 for ubiquitination. Then, Nrf2 migrates to the nucleus, binds to small musculoaponeurotic fibrosarcoma proteins (Maf) and ARE sequences, initiating the transcription of its targeted genes (Cuadrado, 2016; Battino et al, 2018; Robledinos-Antón et al, 2019). In AD, the suggested dysfunction in Nrf2 pathway is supported by Nrf2 age-dependent decreased activity and expression, and by its sustained cytoplasmatic localization, suggestive of a defective nuclear translocation, as previously proved by the team (Mota et al, 2015) and others (Ramsey et al, 2007; Fão et al, 2019; Kaundal et al, 2022).

Accordingly, small molecules with electrophilic properties, such as skin allergens, are capable of dissociating the Keap1 protein, thus promoting Nrf2 translocation to the nucleus (Natsch, 2010) and further transcription of genes participating in detoxification reactions, redox and energy metabolism, inflammation, and proteostasis, all of which are altered in neurodegenerative diseases. In fact, dimethyl fumarate (DMF), a skin allergen known to react with cysteine residues (Natsch et al, 2013), is an orally available disease-modifying agent that was approved by the FDA and EMA as a first-line therapy for the management of relapsing forms of multiple sclerosis (Gold et al, 2022), a disease that shares several pathophysiological characteristics with AD. Importantly, it was recently demonstrated that DMF prevents spatial memory impairments and hippocampal neurodegeneration in rats (Majkutewicz et al, 2016). The well-established effect of skin allergens on the activation of Keap1-Nrf2-ARE regulatory pathway concomitantly with experimental evidences highlighting Nrf2 as an attractive molecular target in the context of AD led us to the straightforward and innovative hypothesis that other skin allergens, never explored in drug discovery programs, when administered by routes other than the skin, may have a positive and therapeutic role in AD, such as Isoeugenol. Isoeugenol (2-methoxy-4-(prop-1-en-1-yl) phenol), is a phenylpropanoid compound present in the essential oils derived from clove (*Eugenia caryophylata*) and an isomer of eugenol (Boulebd, 2019). Isoeugenol is also classified as a moderate cutaneous allergen (Takeyoshi et al, 2008) and an electrophile, with dual activity: prooxidant (by inducing inflammatory responses) or antioxidant (Atsumi et al, 2005). Its structure comprehends a phenolic radical, i.e., a hydroxyl group and an aromatic ring, which is responsible for the double antagonistic activity. The phenolic group is the main structure responsible for free radical scavenging and antioxidant activity (Findik et al, 2011). Accordingly, the antioxidant and anti-inflammatory Isoeugenol properties were previously reported in several animal and cellular models. Isoeugenol was

shown to decrease lipid peroxidation in the liver and brain of normal rats (Rauscher et al, 2001), reduce the levels of NO and ROS in the brain of rats exposed to acrylamide (Prasad and Muralidhara, 2013), inhibit the expression of the inducible nitric oxide synthase (iNOS) proinflammatory enzyme and nitric oxide (NO) levels, in macrophages exposed to lipopolysaccharide (LPS) (Li et al, 2006) and protect against DNA oxidative damage caused by hydroxyl radical, in a molecular simulation model (Wang et al, 2019). In addition, our in-silico data suggested that Isoeugenol displays drug-like properties and capacity to cross the Blood Brain Barrier (BBB) (Silva et al, 2020); thus, this molecule was selected from a physical library of more than 60 skin allergens, to better investigate its effects in an AD context.

Considering the aforementioned, this study evaluated Isoeugenol capacity to revert relevant AD neuropathological events, focused on its antioxidant and anti-inflammatory properties in an AD context. Hence, the antioxidant and anti-inflammatory properties of Isoeugenol were studied in vitro, using an AD neuronal model (N2a neuronal cells, wild type (N2a-wt) and human APP with *Swedish* mutation overexpressing cells (N2a-APPswe)) and a neuroinflammation model (BV-2 mouse microglia cells exposed to LPS), respectively. In vivo studies were also conducted, in APPswe/PSEN1dE9 double transgenic mice (APP/PS1), and their wild-type (WT) counterpart, at an early (6-month-old (mo) mice) and late (11 mo mice) AD stage. Isoeugenol was administrated, during one month, intranasally, which is a simple, fast and non-invasive method for drug delivery into the brain, including of larger molecules that otherwise would not cross the BBB. Moreover, it avoids gastrointestinal metabolization and hepatic first pass effect, allowing lower doses administration thus reducing potential drugs toxicity (Hanson et al, 2013; Fortuna et al, 2014; Serralheiro et al, 2015). As far as we know, we performed for the first-time pharmacokinetic studies concerning Isoeugenol intranasal administration, and a new HPLC method was validated. Qualitative histological studies, neuropathologic markers and mice cognitive function were evaluated.

The results showed that Isoeugenol activated the Nrf2 pathway creating a more favorable antioxidant, anti-inflammatory, metabolic, and proteostasis environment that can limit disease progression. Pharmacokinetic studies demonstrated that Isoeugenol was absorbed and distributed in plasma and brain, following intranasal administration. Moreover, histopathological analysis showed no significant alterations between untreated and treated animals, supporting the safety of Isoeugenol administration. Isoeugenol decreased the levels of Aβ in the brains of APP/PS1 transgenic mice with 6 and 11 mo, as well as Beta-secretase 1 (*Bace1*) gene expression, while increased Heme oxygenase 1 (*Hmox1*) in the hippocampus. Importantly, Isoeugenol improved mice cognition, particularly at 11 mo. Overall, the results

confirmed, for the first time, that Isoeugenol demonstrated a neuroprotective profile in both in vitro and in vivo models of AD, highlighting its therapeutic potential for the treatment of this disease, which should be further explored.

2. Material and Methods

2.1. Materials

Isoeugenol (98% cis and trans racemic mixture), dimethyl sulfoxide (DMSO), Rosewell Park Memorial Institute (RPMI)-1640 medium, lipopolysaccharide (LPS) from Escherichia coli (serotype 026:B6), sodium bicarbonate, L-glutamine and D-(+)-glucose, MEM (Minimum Essential Medium) non-essential amino acid solution, Bovine Serum Albumin (BSA), Bicinchoninic Acid (BCA), penicillin-streptomycin antibiotic, ethylenediamine tetraacetic acid (EDTA), glycerol, Nonidet-P-40, sodium dodecyl sulfate (SDS), protease inhibitor cocktail for *ex vivo* assays, mouse monoclonal anti-β-Tubulin and anti-APP antibodies were obtained from Sigma-Aldrich (St. Louis, MO, USA). Dulbecco's Modified Eagle's Medium (DMEM)-31600 (powder, low glucose with pyruvate; Gibco), geneticin G-418 (Gibco), fetal bovine serum (FBS; Gibco), sodium chloride, Amyloid beta 40 Human ELISA (Invitrogen), Amyloid beta 42 Human ELISA (Invitrogen) and mouse monoclonal anti-HMOX1 antibody were obtained from ThermoFisher Scientific (Walthman, Massachusetts, USA). NZYOL reagent, NZY First-Strand cDNA Synthesis and NZYSpeedy qPCR Green Master Mix (2x) kits were from NZYTech genes & enzymes (Lisbon, Portugal). Nrf2 Transcription Factor Assay colorimetric kit and monoclonal antibodies against pro-IL-1β and lamin B1 were obtained from Abcam (Cambridge, UK). Nuclear Extract kit was purchased from Active Motif. Phosphatase (PhosSTOP) and protease (Complete Mini) cocktail inhibitors were provided by Roche Diagnostics (Mannheim, Germany) and dithiothreitol (DTT) from Roche (Danvers, Massachusetts, USA). Polyvinylidene difluoride (PVDF) membranes were purchased from Millipore Corporation (Bedford, MA, USA). Mouse anti-iNOS monoclonal antibody was obtained from R&D Systems (Mineapolis, MN, USA) and mouse anti-Nrf2 monoclonal antibody from Santa Cruz Biotechnology (Dallas, TX, USA). Mouse phospho-GSK3β, GSK3β, phospho-AKT and AKT monoclonal antibodies, and secondary anti-mouse and anti-rabbit ECL antibodies were obtained from Cell Signaling Technology (Danvers, Massachusetts, USA). Clarity Western ECL (Enhanced Chemiluminescent) Substrate agent was purchased from Bio-Rad Laboratories.

The source of more specific reagents is referred along the text in Methods section 2.2.

2.2. Methods

2.2.1. Blood-Brain Barrier (BBB) Permeability − Parallel Artificial Membrane Permeability assay (PAMPA)

The capacity of Isoeugenol to cross the blood-brain barrier (BBB) was evaluated using a parallel artificial membrane permeability assay (PAMPA) model, as described by our team (Bicker et al, 2016). The reference drugs sulfasalazine, trazodone and propranolol (Sigma-Aldrich, St. Louis, MO, USA) with established BBB permeability were used as control, as follows: sulfasalazine (not permeable (BBB-)), as a negative control; trazodone and propranolol (permeable (BBB+)), as positive controls. The donor solutions of the reference drugs and of Isoeugenol were diluted with phosphate buffer saline (PBS, pH 7.4) to a final concentration of 500 μM for reference drugs, and 150 μg/mL for Isoeugenol (DMSO final concentration = 5%). The 2% (w/v) brain lipid extract solution of porcine polar brain lipid (PBL) (Avanti Polar Lipids, Alabaster, AL, USA) was diluted in n-dodecane (Sigma-Aldrich, St. Louis, MO, USA). The donor solution was prepared by adding 300 μL of the reference drugs or Isoeugenol per well in a microtiter plate (MultiScreen®-IP, catalogue no. MATRNPS50, Millipore Corporation, Bedford, MA, USA). Next, 6 μL of 2% PBL was added to the hydrophobic filter of each acceptor well (MultiScreen®-IP, catalogue no. MAIPNTR10, Millipore Corporation, Bedford, MA, USA) which were then filled with 150 μL of PBS-containing DMSO in the same % of the donor solution. The 96-well microfilter acceptor plate was carefully placed onto the microtiter donor plate and the assembly was incubate for 16 h at room temperature, under gentle stirring. After incubation, the absorbance of the acceptor solutions was read by ultraviolet spectrophotometry, using a SpectraMax Plus 384 Spectrophotometer at the corresponding wavelengths previously determined for each compound, and the necessary dilutions were made to maintain an absorption inferior to 1. Three experiments were executed and the apparent permeability (Papp) of each reference drug and Isoeugenol was calculated applying the equation:

$$\text{Papp} = -2.303 \times \frac{VdnVac}{Vdn + Vac} \times \frac{1}{S \times t} \times \log\left(1 - \frac{flux\%}{100}\right)$$

$$Flux\% = \frac{\text{ODac}}{ODeq}$$

where Vdn is the volume of the donor solution (300 μL), Vac is the volume of the acceptor solution (150 μL), S is the surface area of the filter that separates both compartments (0,26 cm2), t is the incubation time (57 600 s), ODac is the optical density of the acceptor solution and ODeq is the optical density of the equilibrium solution, obtained after the assembly of the two 96-well plares (450 μL). The permeability of

each compound is predicted based on the calculated Papp value, being the cut-off value of 2.0×10^{-6} centimeters per second (cm s-1).

2.2.2. β-site APP cleaving enzyme 1 (BACE1) Activity Assay

The β Secretase 1 (BACE1) Activity Detection Kit CS0010 (Sigma-Aldrich Co. LLC., St. Louis, MO, USA) allows a screening of BACE1 inhibitor molecules based on a 45-fluorescence resonance energy transfer method that is observed when there is cleavage of the substrate by the enzyme. BACE1 substrate stock solution (500 µM) was prepared in DMSO, aliquoted and stored at –20 °C. Just before the beginning the assay aliquots of BACE1 substrate and of the enzyme solution were brought to room temperature, and further diluted with the fluorescent assay 10-fold to a final concentration of 50 µM and 0.3 unit/µL, respectively, and kept in ice. A solution with an inhibitor provided with the kit was prepared in DMSO (1 mM) and then diluted to a concentration of 750 nM. Isoeugenol was tested at 50, 100 and 250 µM. The components were added to a 96 wells plate (according the manufacturer's instructions). Blanks (without the addition of the enzyme and substrate and with Iso) were also prepared to evaluate the fluorescence of the test compound per se in the aforementioned concentrations. The plate was incubated for 2 hours at 37 °C and the fluorescence read in a fluorimeter at 320 nm (excitation) and 405 nm (emission) with an automatic cut-off of 325 nm. Final fluorescence values were calculated by subtracting the negative control (with substrate and no enzyme) and the respective blank fluorescence to that of the tested compound, and expressed as % of the positive control (considered as 100% of BACE activity). Results are shown as mean of the obtained percentage of inhibition (%) ± standard error of the mean (SEM) for the three experiments performed in duplicate and were calculated by comparison with the positive control. β-Secretase Inhibitor IV (Calbiochem, Merck KGaA, Darmstadt, Germany) was used as a reference inhibitor at its IC_{50} concentration (15 nM) to validate the procedure.

2.2.3. Cell culture and treatment

The neuronal mouse neuroblastoma cell lines (N2a) wild-type (N2a-wt; Neuro2a (ATCC® CCL131™) from American Type Culture Collection) and human Swedish-mutant APP695 (N2a-APPswe; a gift from Dr. Ciro Isidoro, Università del Piemonte Orientale "A. Avogadro", Novara, Italy) were cultured in DMEM-31600 medium supplemented with 3.7 g/L sodium bicarbonate, 4.5 g/L D-glucose, 1% (v/v) non-essential amino acids and 10% (v/v) FBS inactivated at 56 °C for 30 min. N2a-wt cells were further supplemented with 1% (v/v) penicillin-streptomycin and the N2a-APPswe cells with 0.4 mg/mL geneticin G-418.

The murine microglia cell line (BV-2; obtained from Interlab Cell Line Collection (ICLC ATL03001)) were cultured and maintained in RPMI-1640 medium supplemented with 10% (v/v) FBS (inactivated at 56 °C for 30 min), 1% (v/v) penicillin-streptomycin, 2 g/L sodium bicarbonate and 2 mM L-glutamine.

All cell lines were subcultured every 2-3 days and maintained at 37 °C in a 5% CO_2 atmosphere.

N2a cells were plated at a density of 5.3 x 10^4 cells/cm^2 and BV-2 cells were plated at a density of 2.5 x 10^4 cells/cm^2 and allowed to stabilized overnight (ON). N2a-wt and BV-2 cells were exposed to different concentrations of Isoeugenol (in µM: 500, 250, 100, 50 e 5) for 24 h and cell metabolic capacity evaluated by the resazurin assay (as explained in Supplementary Method S1). Accordingly, Isoeugenol non-toxic concentration used in vitro was 250 µM (Supplementary Fig. S1) (in DMSO – up to a concentration of 0.1% (v/v)).

N2a cells: The cells were treated with Isoeugenol for 24 h for quantification of $A\beta_{40}$ and $A\beta_{42}$ peptides levels and for determination of HMOX1 protein levels; for 2, 4 and 6 h for Nrf2 nuclear levels and activation; for 1, 3 and 6 h for analysis of *Hmox1* gene expression and for 5, 15 and 30 min for quantification of the phosphorylated (p) levels of AKT and GSK3β proteins.

BV-2 cells: The cells were stimulated with LPS (50 ng/mL, in sterile PBS), added 30 min after Isoeugenol treatment, in a total of 18 h for gene expression analysis (*Nos2, Il-1β*) or in a total of 24 h for protein levels analysis (iNOS and pro-IL-1β) and for quantification of the extracellular levels of IL-1β and nitrites.

2.2.4. Animals' maintenance

APP/PS1 double-transgenic (B6C3-Tg (APPswe/PSEN1dE9)85Dbo/Mmjax) mice were obtained from Mutant Resource and Research Center (MMRC) – Jackson Laboratory (Bar Harbor, ME, USA). The in-house colony at Centre for Neuroscience and Cell Biology (CNC), University of Coimbra, was maintained in a hemizygote state by crossing transgenic male mice to B6C3F1/J female mice provided from Charles River Laboratories (France). The APP/PS1 mice and the age-matched Wild-Type (WT) littermates, were kept under standard conditions in individually ventilated cages, under standard conditions of temperature (22 °C ± 3 °C) and humidity (50-60%) on a 12 h light/dark cycle and with free access to water and food (Breeding diet A03, Barcelona). The experiments were performed in the light phase of the circadian cycle. All procedures involving animals were in accordance with the European Community guidelines for the use of animals in a laboratory (Directive 2010/63/EU) and were approved by the Direção

Geral de Alimentação e Veterinária (DGAV; Ref: 0421/000/000/2021) and performed by users licensed by the Federation for European Laboratory Animal Science Association (FELASA).

2.2.4.1. 5-6 month-old females – in vivo procedures and sample collection

Five month-old (mo) females were intranasally administered with Isoeugenol (50 mg/kg, in sterile PBS), daily, for a period of one month. The animals were subdivided into the following groups: 6 WT mice administered with PBS (WT VEH, as disease control); 5 APP/PS1 mice administered with PBS (APP/PS1 VEH, as vehicle control); 5 APP/PS1 mice administered with Isoeugenol (APP/PS1 Iso). Intranasal administration was performed without anesthesia, using a micropipette and according to the protocol by Hanson et al (2013). Before administration, the animals had a period of conditioning to handling for the performance of the technique. The administered volume was 6 µL per nostril, making a total of 12 µL. The animals were sacrificed under anesthesia with 4% of isoflurane in an induction chamber, followed by decapitation for total blood collection and the brain was quickly dissected and frozen in iced-nitrogen. The blood collected to Vacuette K3EDTA tubes (Greiner Bio-One, Kremsmünster, Austria) was centrifuged at 1000 g for 15 min at 4 °C. The aliquoted samples were stored at -80 °C until their use. Biological samples (brain and blood) were collected for neurochemical analysis of AD biomarkers and evaluation of the metabolic parameters (triglycerides and glycemia), respectively.

2.2.4.2. Pharmacokinetic studies

Pharmacokinetic studies were performed in WT mice with the same background (B6C3F1) of transgenic APP/PS1 mice. Mice (25-30 g) were housed in local animal facilities under controlled conditions as previously mentioned, for at least 7 days before experiments, with ad libitum access to standard rodent diet and tap water.

Mice (n = 24) were randomly divided into 6 groups (n = 4), representing 6 time-points (5, 15, 30, 60, 120 and 180 min) and anesthetized with a mixture of ketamine (100 mg/kg) and xylazine (10 mg/kg) by intraperitoneal route to ensure their immobility during Isoeugenol (100 mg/kg, dissolved in sterile PBS) intranasal administration. Intranasal administration followed procedures previously established by team members (Gonçalves et al, 2019, 2021; Silva et al, 2021). Briefly, 15 µL of Isoeugenol were instilled into the left nostril with a polyurethane tube (24G x 19 mm) attached to a 1 mL syringe, while the animal was positioned in lateral decubitus. Mice were sacrificed by cervical dislocation and decapitation, and blood was immediately collected into heparinized tubes and centrifuged (1250 g at 4ºC for 10 min) to obtain

plasma samples. Brain and lungs were excised, washed with sodium chloride 0.9% solution, dried and weighed. The samples were stored at -80 °C until analysis by a high-performance liquid chromatography (HPLC) method, validated according to international guidelines (Guideline M10 on Bioanalytical Method Validation; ICH, 2019) (Supplementary Table SI). Tissues were homogenized with NaCl 0.9% (brain: 3 ml/g of tissue; lung: 4 mL/g of tissue) using a tissue homogenizer with a Teflon® pestle from Thomas Scientific (Swedesboro, NJ, United States). This was followed by centrifugation (1803 g at 4°C for 15 min) and supernatant analysis by HPLC (Supplementary Methods S2 and S3).

Mean experimental concentration versus time profiles were plotted in plasma, brain and lung, and submitted to non-compartmental pharmacokinetic analysis, using WinNonlin software, version 5.2 (Pharsight Co, Mountain View, CA, USA). The following pharmacokinetic parameters were obtained in plasma and tissues: maximum concentration (Cmax); time required to reach Cmax (tmax); area under the concentration-time curve from time zero to the time of last measurable concentration (AUCt), and from time zero to infinity (AUCinf); extrapolated area under the concentration-time curve (AUCextrap); elimination rate constant (Kel); and apparent elimination half-life (t1/2β). Brain/plasma and lung/plasma ratios were also determined, in order to compare tissue and systemic exposures.

2.2.4.3. Biochemical and histological analyses

The safety of Isoeugenol was evaluated in an additional group of 10 mo WT female mice (from the same littermate as the males further used). For that, awake animals were again daily administered intranasally with Isoeugenol (n=3), or PBS (n=4) for 28 days. After treatment and after a 6 h fast, the animals were anesthetized with 100 mg/kg ketamine and 10 mg/kg xylazine, the blood was collected by cardiac puncture into serum tubes with clot accelerator, and granule serum separator, allowed to clot for 30 min, and centrifuged at 4,000× *g* for 20 min at RT. Metabolic parameters, namely glucose, triglycerides, cholesterol, high-density lipoprotein (HDL), and low-density lipoprotein (LDL) cholesterol levels were evaluated by spectrophotometric determination of chemical reactions in a Autoanalyser [(ARCHITECT ci-1000 Chemistry Analyzer (Abbott Laboratories, Chicago, IL, USA)] at the Clinical Analysis Laboratory at the University of Coimbra. In addition, markers of liver (glutamic-oxaloacetic transaminase (GOT), gamma-glutamyl transferase (GGT), and alkaline phosphatase (ALP)), and kidney (albumin, creatinine, and urea) function were also measured using the same technique to discard hepatic and renal toxicities. The results were expressed as the amount of the parameter in milligrams per deciliter or international units per liter detected in the serum of the animals. To detect any significant tissue changes, a

histopathological analysis of excised lung, kidney, brain, heart, and liver tissues was conducted. After blood collection, the animals were perfused by cardiac route with PBS, and 4% (w/v) paraformaldehyde (PAF) solution in PBS. The organs were removed and fixed for 24 h in PFA solution at 4 °C and then stored in PBS (pH 7.4) containing 0.1% (w/v) sodium azide at 4 °C until processing. After cardiac perfusion, a small incision was made on the ventral surface of the trachea, where the sheath of a 20 G angiocatheter was slid to insufflate the lungs with 1 mL of PBS, and 1 mL of the PAF. The lungs were collected and stored in PAF at room temperature until histological analysis (as previously performed by the team) (Gonçalves et al, 2019). Then, series of gradient concentrations of ethanol were used to dehydrate the specimens, followed by xylene clearing and impregnation in paraffin. After, tissue sections (4 µm) of lung, kidney, brain, heart and liver were embedded in paraffin and stained with hematoxylin and eosin (H&E) (according to Ruehl-Fehlert et al, 2003). Images were obtained using a Leica DM1000 LED microscope (Leica Microsystems, Wetzlar, Germany) and blind-analyzed by an expert pathologist.

2.2.4.4. 10-11 month-old males – in vivo procedures and sample collection

Ten mo males APP/PS1 double-transgenic mice and age-matched WT littermates, from our in-house colony (Centre for Neuroscience and Cell Biology (CNC), University of Coimbra), were housed in local animal facilities under controlled conditions as previously mentioned. Animals were randomly divided into 4 groups (n = 6-8/group): WT Vehicle (VEH) and APP/PS1 Vehicle (VHE), submitted to PBS via intranasal administration for 28 days; WT Isoeugenol (Iso) and APP/PS1 Isoeugenol (Iso), submitted intranasally to 100 mg/kg/day Isoeugenol (emulsified in PBS) for 28 days. The PBS or Isoeugenol administration followed the methodology for intranasal administration of CNS therapeutics to awake mice described by Hanson et al. (2013). Body weight was monitored during treatment and in the day before the end of treatment the intraperitoneal glucose tolerance test (ipGTT) was performed after a 6 h fast using 1.8 mg glucose per kg body weight and the evaluation of glycaemia was performed at 0, 15, 30, 60 and 120 min using a glucose meter and test strips (Contour, Bayer, Leverkusen, Germany). Response to glucose was expressed by area under the curve (AUC). Serum triglycerides were measured in the same day before glucose administration (Accutrend Plus Meter mg/dl, Roche, Basel, Switzerland). In the next day, two hours after the last dose of Isoeugenol animals were then sacrificed by cervical dislocation after being anesthetized with 4% of isoflurane in an induction chamber. Total blood was collected to Vacuette K3EDTA tubes (Greiner Bio-One, Kremsmünster, Austria) and the plasma was obtained after centrifugation at 1,000× g for 15 min at 4 °C, and stored at -80 °C until use. The brain of each animal was removed, the cerebral cortex and the hippocampus were dissected, and the samples were immediately

frozen, and stored at – 80 °C. Lungs, liver and kidney, were also collected and immediately frozen and stored at –80 °C until use.

2.2.5. Nitric oxide production

Nitric oxide (NO) production was measured in the supernatants of treated BV-2 cells (as described in the "Cell treatment" section), using the Griess assay (Green et al, 1982). Equal volumes of culture supernatants of BV-2 and Griess reagent (1% (w/v) sulphanilamide, 5% (w/v) phosphoric acid and 0.1% (w/v) N-(1-naphtyl)-ethylenediamine dihydrochloride) were mixed and incubated for 10 min, at RT in the dark. Next, the absorbance was read at 550 nm in Biotek Synergy HT (Biotek, Winooski, VT, USA) plate reader and the nitrite concentration of each sample was extrapolated from a standard curve of sodium nitrite.

2.2.6. Aβ40 and Aβ42 peptide levels quantification

Quantification of Aβ40 and Aβ42 peptide levels in cells and animals' biological samples was performed using the Amyloid beta 40 Human ELISA kit and the Amyloid beta 42 Human ELISA kit, respectively and following the manufacturer's instructions. The absorbance was read at 450 nm in a Biotek Synergy HT plate reader (Biotek, Winooski, VT, USA) and the peptide concentration (in pg/mL) was determined according to an Aβ standard curve.

2.2.7. Gene expression analysis by real-time RT-PCR

Total RNA was extracted with NZYol reagent and RNA concentration was quantified using a NanoDrop spectrophotometer (Thermo Scientific, Wilmington, DE, USA). Samples were stored at –80 °C in an RNA storage solution until use. 2 µg of RNA were transcribed to cDNA (using the NZY First-Strand cDNA Synthesis kit) in a C1000 Thermal Cycler (Bio-Rad). The resulting products were amplified in duplicate with NZYSpeedy qPCR Green Master Mix (2x) kit by real-time RT-PCR in a CFX Connect Real-Time System (Bio-Rad). After amplification, a threshold for each gene and Ct (Cycle threshold) were calculated and normalized using *Hprt-1* (Hypoxanthine-guanine phosphoribosyl transferase) as reference gene. The results were analyzed using Bio-Rad CFX Maestro 1.1 system software (Hercules, CA, USA). Mouse forward (F) and reverse (R) primers were designed with Beacon Designer software version 7.7 (Premier Biosoft International, Palo Alto, CA, USA) and synthetized by Eurofins (Eurofins Scientific, Luxembourg, Luxembourg) or purchased from Sigma (Sigma-Aldrich, St. Louis, MO, USA), as follows:

Il1β (F: TCTATACCTGTCCTGTGTAATG and R: GCTTGTGCTCTGCTTGTG3); *Trem2* (F: CAGGAATACTGGTGTGTA and R: TGTGGAGAATGTTTAATGTC); *Hmox1* (F: CCAGTTCTACCAGAGTAA and R: ACAGAAGTTAGAGACCAA); *Bdnf* (F: CCACTAAGATACATCATAGC and R: CAGAACAGAACAGAACAG); *Hprt1* (F: GTTGAAGATATAATTGACACTG and R: GGCATATCCAACAACAAAC) (Eurofins).

Nos2 (F: GCTGTTAGAGACACTTCTGAG and R: CACTTTGGTAGGATTTGACTTTG); *H-APP* (F: ATTGCCAAGAAGTCTACCC and R: AGTTCTGGATGGTCACTG); *Bace1* (F: GAAGTGATCATTGTACGTGTG and R: TCTTGTCGTAGTTGTACTCC); *Ppargc1α* (F: TCCTCTTCAAGATCCTGTTAC and R: CACATACAAGGGAGAATTGC); *Prkcg* (F: CCTTTCTGTGTTCTAGATTCC and R: GCATAAAACTACCAAGTGGG); *Aif/Iba1* (F: TTCATCCTCTCTCTTCCATC and R: TCAGCTTTTGAAATCTCCTC) (Sigma-Aldrich);

Since the results are presented as ratios of treated samples/untreated (control) cells, a two–base logarithmic transformation was used to make observations symmetric and closer to a normal distribution. If x represents the gene fold change in one sample, then the two–base logarithmic transformation ($\log_2(x)$) is $\ln(x)/\ln(2)$. Hence, fold changes of 2 and 0.5 correspond to mean $\log_2$ values of 1 and –1, respectively.

2.2.8. Protein extracts and quantification

Total cell extracts were obtained by incubated the cells pellet (after washed in ice–cold PBS (pH=7.4) and centrifuged at 300 *g* for 5 min at 4 °C) in RIPA lysis buffer (150 mM sodium chloride, 50 mM Tris–HCl (pH=8.0), 2mM EDTA, 0.5% (w/v) sodium deoxycholate, 0.1% (w/v) SDS and 1% (v/v) Nonidet P-40), supplemented with 1 mM dithiothreitol and phosphatase (1:10) and protease (1:7) inhibitors, for 30 min in ice. After, samples were centrifuged at 12 000 *g* for 10 min at 4 °C and the supernatant fraction was collected and stored at –80 °C until use.

Cell nuclear and cytoplasmatic extracts were obtained with a commercial kit (Nuclear Extract kit), following the manufacturer's instructions. The extracts were stored at –80 °C until use.

Protein concentration was determined using the bicinchoninic acid method extrapolated from a protein standard curve (BSA). Lysates were denatured in 4x concentrated loading buffer (0.25 M Tris (pH=6.8), 4% (w/v) SDS, 200 mM DTT, 20% (v/v) glycerol and bromophenol blue), for 5 min at 95 °C.

2.2.9. Protein levels analysis by Western Blotting

The corresponding 30 μg of denatured protein was electrophoretically separated on 10% (v/v) sodium dodecyl sulphate–polyacrylamide gels (SDS-PAGE) at 130 V. After, proteins were electrotransferred onto PVDF membranes using a wet transfer system (Bio-Rad, USA) at 350 mA, for 210 min at 4 °C. After, membranes were blocked with 5% (w/v) of non-fat dry milk or bovine serum albumin (BSA; for phosphorylated forms), diluted in Tris-buffered saline [(TBS): 150 mM NaCl, 25 mM Tris-HCl (pH=7.6) with 0.1% Tween-20 (TBS-T)], for 1 h at room temperature (RT). Then, membranes were incubated with the primary antibodies against: HMOX1 (1:500), iNOS (1:500), pro-IL-1β (1:1000), Nrf2 (1:500), diluted in PBS and pAKT/AKT (1:1000) and pGSK3β/GSK3β (1:1000) diluted in BSA, ON at 4 °C. Membranes were washed 30 min with TBS-T and incubated with the respective secondary antibodies: anti-mouse horseradish peroxidase conjugated secondary antibody (1:1000) or anti-rabbit horseradish peroxidase conjugated secondary antibody (1:1000), for 1 h at RT. After washing with TBS-T (10 min x 3), membranes were incubated with the loading control proteins: Lamin B1 (1:1000) for nuclear extracts or β-Tubulin (1:20 000), for total or cytoplasmatic extracts, during 1 h at RT. Immune complexes were detected with Clarity Western ECL (Enhanced Chemiluminescent) Substract and the blots were visualized by chemiluminescence using ImageQuant TM LAS 500 (GE, Healthcare, Chicago, Illinois, USA) image system. The blots images were analyzed using TotalLab TL120 (Nonlinear Dynamics Ltd., Newcastle upon Tyne, UK).

2.2.10. Nrf2 activation

The N2a-wt and N2a-APPswe cells were treated as described in the "Cell treatment" section with exception of the solvent used (ethanol, due to DMSO-induced increase in Nrf2 nuclear expression (data not shown)). Briefly, 5 μg of protein from nuclear extracts were used to assess Nrf2 activation using a commercial kit (Nrf2 Transcription Factor Assay Kit), according to manufacturer's instructions. The absorbance was read at 450 nm and 665 nm (reference wavelength) in a spectrophotometer and the activation of Nrf2 was calculated relatively to the positive control provided with the kit.

2.2.11. Behavioural experiments

The behavioural tasks "Hot plate" and "Open field" were performed to ensure animal equivalence between experimental groups, in terms of pain sensitivity and locomotor activity, respectively.

The "Elevated plus maze" was done to evaluate animals' anxiety level. The modified "Y-maze" and "Novel object recognition" tasks, which relies on the innate preference of rodents to explore novelty, were performed as a measurement of short-term spatial and social recognition memory, respectively, and "Fear condition" test to evaluate the hippocampal–dependent long-term contextual/associative memory.

All the behavioural tests were performed during the light phase of the circadian cycle (between 9.00 am – 5.00 pm), under red/low light. The intranasal administration of VHE or Isoeugenol was performed around 6.00 pm, to avoid the repercussion of the acute effect of the drug in the behavioural tasks and in the animal sleeping cycle. For all the tests, mice were acclimated into the test room for a 1 h period. Between each trial the apparatus was cleaned with a 10% ethanol solution to avoid odour cues. All experimental data was analysed using the ANY-maze video tracking system, Stoelting, US.

Hot plate test

The hot–plate test (LE7406 Hot-Plate, Panlab, Barcelona, Spain) evaluates thermal pain reflexes due to footpad contact with a heated surface. During the experiments, the animal was placed on a thick aluminium plate (10 mm) at 55 ^{o}C and confined in a removable clear acrylic cylinder where the latency time to the first hind paw or/and jumping responses were measured.

Open field

Mice were placed in a 42×42 cm arena with 42 cm high walls and they were allowed to explore for 10 min. The time spent on the central and peripheral zones of the chamber, the number of entries in each one of them and the values of mean speed and total distance travelled were analysed.

Elevated plus maze

The apparatus was composed of two open arms and two enclosed arms (30 × 5) with 15 cm high wall arranged so that the arms of the same type are opposite to each other with a central square of 5 cm. The apparatus was elevated to a height of 50 cm above floor level. The trial involved placing the individual animal on the central platform of the maze facing an open arm. Number of entries and the time spent in closed and open arms were recorded for a 5 min test. Entry into an arm was defined as the animal placing all four paws onto the arm.

Y-maze.

The Y-maze apparatus, made from impermeable black formica, consisted of three arms (30 cm long, 20 cm height and 5 cm large) placed at 120° with respect to each other. Arms were equipped with different internal visual cues placed on the side and end walls of each arm. During the training phase, one arm was

blocked by a removable door. In this phase the mice were positioned in the start arm, facing the centre of the maze and allowed to explore only two arms (start and other) for 8 min. The test was performed 2 hours later (with the door blocking the novel arm removed) and the animals were placed again in the start arm and allowed to explore the three arms during 8 min. The number of entries and the time spent in novel arm was measured.

Novel Object recognition

Firstly, the mice were habituated for a 10-min period in the empty chamber during the open field test. Then, in the training phase, performed 1 h after the habituation phase, two identical 200 mL brown glass bottles were placed 15 cm away from the walls of the arena. The mice were placed at the centre of the apparatus and allowed to explore these two identical objects for 10 min, and we recorded the time spent sniffing/whisking or looking (≤ 1 cm) at the objects. The test was performed 1h and 30 min later, where one of the objects was replaced by a 50 mL volumetric flask filled with dyed sterile water with the same diameter creating a novelty for the animal to explore during 5 min; again, the time spent exploring both the novel and the familiar objects was recorded. The recognition index was determined by the percentage of time spent investigating the novel object over the time spent exploring both objects.

Fear conditioning

Fear conditioning is a form of associative learning that occurs when a previously neutral stimulus (e.g. tone) elicits fear responses after it has been paired with an aversive stimulus (e.g. electric paw shock). Firstly, on day one (training day), the mice were submitted individually to an A context, and after 2 min of habituation, to two presentations of an auditory conditioned stimulus (95 dB for 30s), paired with a paw shock unconditioned stimulus (0.5 mA for 2s), applied at the end of the auditory stimulus, with a 60s interval between presentations. One minute after the last pair of auditory–shock stimuli, the animals were placed back in the housing cage. On day two (contextual memory) mice were returned to context A in the conditioning chamber and "freezing" behaviour was measured over a period of 5 minutes. On the third day (associative memory) animals were placed in a different context B (conditioning chamber with perspex floor and walls with different patterns from those of context A and change of lighting) and "freezing" behaviour was measured over a period of 3 min, after which the auditory stimulus was introduced for a further 3 min, during which the "freezing" behaviour was also evaluated.

2.2.12. Statistical analysis

Results are presented as mean ± SEM of the number of experiments performed and were analyzed with ANOVA, followed by a Dunnet's or Tukey's multiple comparison post-test or Unpaired *t*-test for comparisons between two groups. The *in vitro* results were compared relative to untreated cells (Ctr). Comparisons between Ctr and the vehicle (DMSO) were performed and differences not detected (unless otherwise stated, as in *Nrf2 activation* section). The *in vivo* results were compared relative to healthy animals of the control group (WT) or transgenic control group (APP/PS1). GraphPad Prism 8.0.2 (GraphPad Software, San Diego, CA, USA) was used to perform the statistical analysis of the results. A value of p<0.05 was considered significant.

3. Results

3.1. Isoeugenol crosses the BBB and inhibits BACE activity in chemico

First, we performed in chemico experiments to evaluate Isoeugenol (Iso) ability to cross the BBB and to inhibit BACE1 enzyme activity. In order to explore the capacity of Iso to cross the BBB and penetrate into the brain, the PAMPA assay was used. Iso permeability was determined through the lipid membrane extract, together with three reference compounds (Fig. 1). The results suggested that Iso can cross the BBB, corroborating our previous obtained in silico results (Silva et al, 2020).
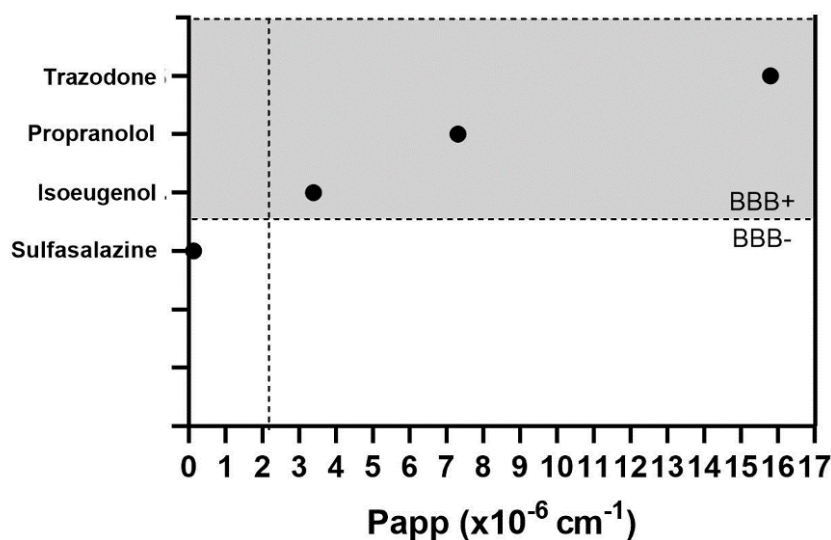
Fig. 1. Blood-brain barrier (BBB) permeability of Isoeugenol. Iso permeability through BBB, expressed as experimental Papp (Permeability coefficient through the artificial membrane) values obtained with PAMPA models with 2% (w/v) porcine polar brain lipid (PBL). Data represent the mean of Papp in centimeters per second of three independent experiments performed in duplicate. Legend: (BBB-), non-BBB permeable; (BBB+), BBB-permeable. Iso — Isoeugenol

Concerning BACE1 activity and according to Table I, Iso–induced inhibition of BACE1 activity is dose-dependent reaching nearly 40% at the higher concentration tested (250 µM).

Test Compound	Concentrations			
	15 nM	50 µM	100 µM	250 µM
Isoeugenol		27.80 ± 10.02	31.07 ± 15.25	38.28 ± 6.74
β-Secretase Inhibitor IV*	47.5 ± 2.09*			

Table I. BACE1 activity inhibition induced by Isoeugenol.

Values correspond to the average percent inhibition for each of the concentrations tested and are presented as the mean ± SEM of three independent experiments performed in duplicate.

*Inhibitory activity close to 50%, as expected for the concentration used (15 nM), corresponds to the IC_{50} value reported in the literature (Coimbra et al., 2020).

3.2. Isoeugenol reduces Aβ40 peptide levels in an AD cell model

To select the non-toxic concentration of Iso to be further used, the metabolism of microglial (BV-2) and neuronal (N2a-wt) cells were evaluated by Alamar Blue assay (resazurin) after cells exposure to different concentrations of Iso (500 μM, 250 μM, 100 μM, 50 μM and 5 μM) for 24 h (see Supplementary Method S1 and Fig. S1). Considering untreated cells as 100% metabolically active, we selected the concentration of 250 μM of Iso, since it was the highest concentration tested that did not induce alterations in N2a-wt (98.5%) or BV-2 (96.5%) cells metabolic activity.

To validate and support the APP-overexpressing cells with Swedish mutation (N2A-APPswe) as an AD model, we measured the levels of Aβ40 and Aβ42 peptides that lead to the formation of senile plaques, which is one of AD hallmarks. Peptides levels were quantified by ELISA, in the supernatants of N2a-wt and N2a-APPswe cells (exposed or not to Iso for 24 h) (Figure 2).
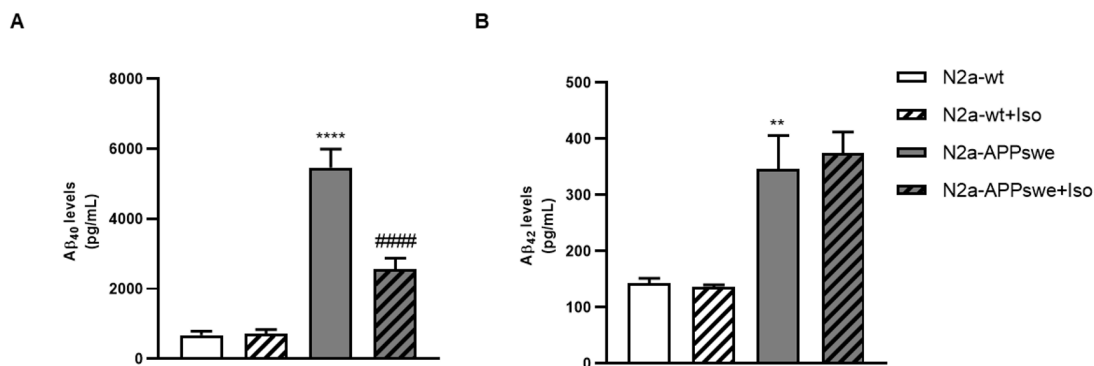
Fig. 2. **Effect of Isoeugenol on Aβ peptides levels in neuronal cells.** $A\beta_{40}$ (A)and $A\beta_{42}$ levels (B)in N2a-wt and N2a-APPswe cells exposed to Iso. Data correspond to the mean ± SEM of four to sixindependent experiments. Statistics: One-way ANOVA with Tukey's multiple comparisons test. $p < 0.05$ was considered significant. ** p < 0.01 and **** p < 0.0001, compared to N2a-wt; #### p < 0.0001, compared to N2a-APPswe. Legend: Iso – Isoeugenol

As expected, N2a-APPswe cells secreted higher levels of Aβ40 (~8 fold-increase; p < 0.0001; Fig. 2A) and Aβ42 (~2.4 fold-increase; p < 0.01; Fig. 2B) peptides, when compared to N2a-wt cells. Moreover, Iso

treatment significantly decreased Aβ40 peptide levels (Fig. 2A), compared to untreated cells (N2a-APPswe) although no effect was observed in Aβ42 peptide levels (Figure 2B).

3.3. Isoeugenol activates Nrf2 pathway in an AD cell model − involvement of AKT/GSK3β pathway

As an electrophilic molecule, Iso is expected to react with cysteines in Keap1 protein and lead to Nrf2 release and further nuclear translocation and activation. Nevertheless, we wanted to explore if AKT/GSK3β pathway was also affected by Iso treatment. Hence, we exposed N2a-APPswe cells to Iso for 5,15 and 30 min and AKT and GSK3β phosphorylated levels were determined by western-blotting (WB) (Fig. 3).
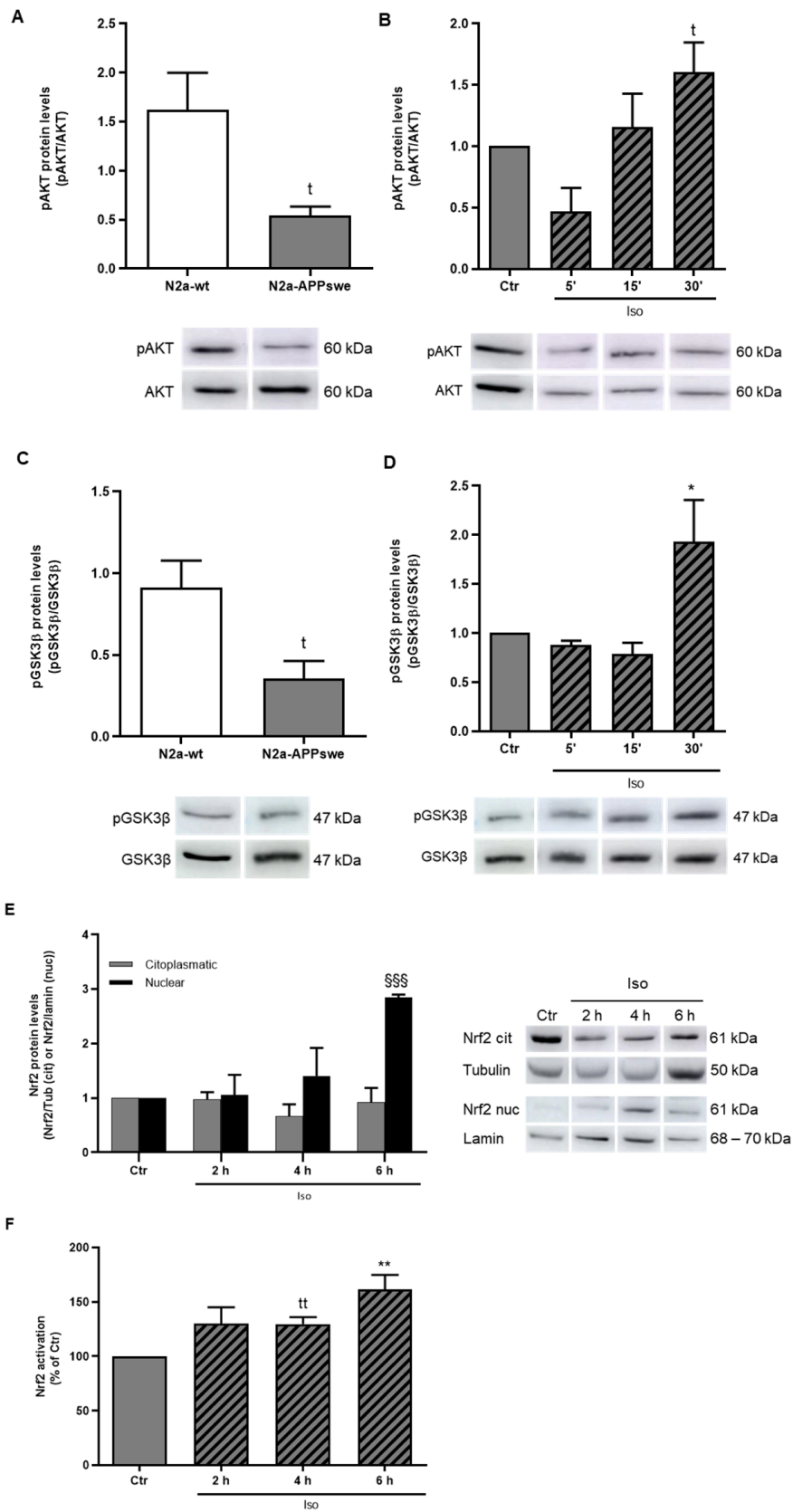
Fig. 3. Effect of Isoeugenol on AKT, GSK3β and Nrf2 activation in AD neuronal cells. WB analysis of AKT (A, B) and GSK3β (C, D) phosphorylated (p) protein levels, and of cytoplasmatic and nuclear Nrf2 (E) levels, in N2a-APPswe cells exposed to Iso for 5, 15 or 30 min (B, D) or for 2, 4 and 6 h (E). Nrf2 activation determined in N2a-APPswe cells after 2, 4 and 6 h of Iso exposure (F), using a commercial kit. The basal levels of pAKT and pGSK3β in untreated N2a-wt and N2a-APPswe neuronal cell lines are depicted in (A) and (C), respectively, determined at the longest time-point evaluated (30 min). Representative blot images are presented. Values are the mean ± SEM of three to four independent experiments and expressed relatively to control (Ctr) cells. Statistics: Unpaired t-test (t), one-way ANOVA with Dunnett's multiple comparisons test (*) and two-way ANOVA with Sidak's multiple comparisons test (§). $p < 0.05$ was considered significant. (t) and (*) $p < 0.05$, compared to N2a-wt (A, C) or Ctr cells (B, D); (tt) and (**) $p < 0.01$ and §§§ $p < 0.001$, compared to Ctr cells. Legend: Iso − Isoeugenol; Nrf2 cit − Nrf2 cytoplasmatic levels; Nrf2 nuc − Nrf2 nuclear levels.

As we can observe, both AKT (Fig. 3A) and GSK3β (Fig. 3C) phosphorylated levels are significantly reduced in N2a-APPswe cells (compared to N2a-wt), suggesting a defective AKT activation and GSK3β overactivation, with consequent Nrf2 retention in the cytoplasm. Interestingly, Iso induced AKT activation (Fig. 3B) resulting in GSK3β inactivation (Fig. 3D), in N2a-APPswe cells exposed to Iso for 30 min. Next, we aimed to confirm if Nrf2 activation was in fact induced by Iso. Therefore, we further analyzed Nrf2 cytoplasmatic (Nrf2 cit) and nuclear (Nrf2 nuc) levels by WB, and Nrf2 activation (by a colorimetric kit), in N2a-APPswe cells, exposed to Iso for 2, 4 and 6 h (Figs. 4E and 4F, respectively). According to the results, Nrf2 nuclear levels were significantly increased in N2a-APPswe cells exposed to Iso for 6 h, compared to the control (Ctr; N2a-APPswe untreated cells), suggesting its nuclear translocation and activation, as corroborated by the results obtained with the colorimetric kit (Fig. 4F).

3.4. Isoeugenol increases Hmox1 gene expression and HMOX1 protein levels in an AD cell model

We further analyzed the effect of Iso on ARE-Nrf2-dependent *Hmox1* gene expression (by real time RT-PCR) and HMOX1 protein levels (by WB), in N2a-APPswe cells exposed to Iso for 1, 3 and 6 h (Figs. 4A–B) or 24 h (Figs. 4C-D).
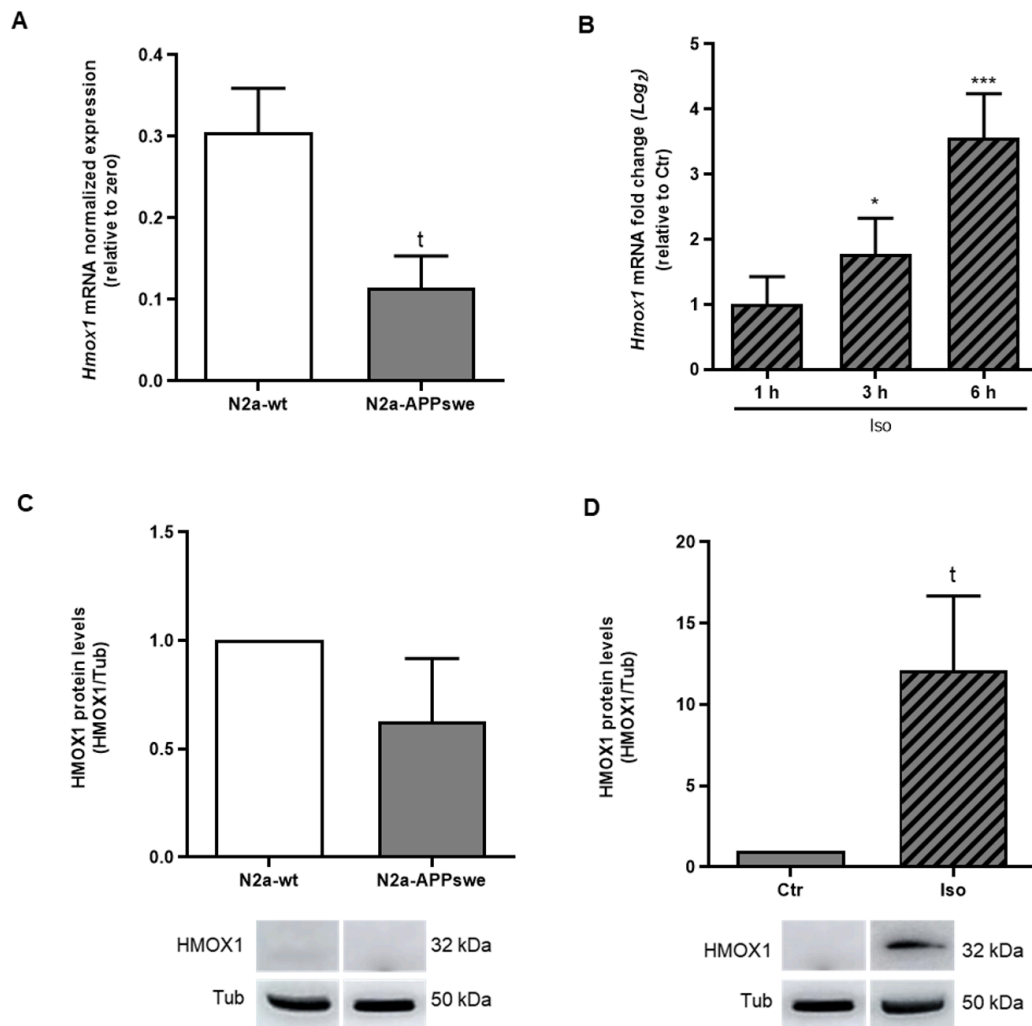
Fig. 4.Effect of Isoeugenol on Nrf2-dependent antioxidant *Hmox1* gene expression and HMOX1 protein levels in AD neuronal cells.*Hmox1* mRNA levels were determined by real–time RT-PCR, in N2a–APPswe cells exposed to Iso for 1,3 and 6 h (A, B). HMOX1 protein levels were determined by WB, in N2a–APPswe cells exposed to Iso for 24 h (C, D). Representative blot images are presented. The basal levels of *Hmox1* gene and HMOX1 protein in untreated N2a–wt and N2a-APPswe neuronal cell lines are depicted in (A) and (C), respectively, determined at the longest time-point evaluated. Values are the mean ± SEM of four to six independent experiments and expressed relatively to control (Ctr) cells. Statistics: Unpaired t-test (t) and one–way ANOVA with Dunnett′s multiple comparisons test (*). $p < 0.05$ was considered significant. (t) and (*) $p < 0.05$, compared to N2a–wt (A) or Ctr cells (D); *** $p < 0.001$, compared to Ctr cells ($Log_2 1=0$). Legend: Iso − Isoeugenol.

Hmox1 gene expression is reduced in N2a–APPswe cells (compared to N2a–wt) and was significantly increased by Iso, after 3 and 6 h of cell exposure, with an increase in HMOX1 protein levels, after 24 h, in N2a–APPswe cells, compared to control (Ctr). These results highly suggest that the Nrf2–dependent antioxidant via is activated by Iso in an AD context.

3.5. Isoeugenol reduces pro-inflammatory parameters in a neuroinflammation cell model

To study the effect of Iso on neuroinflammation, LPS–stimulated microglia was treated with Iso and the production of pro-inflammatory mediators was evaluated (Fig. 5).
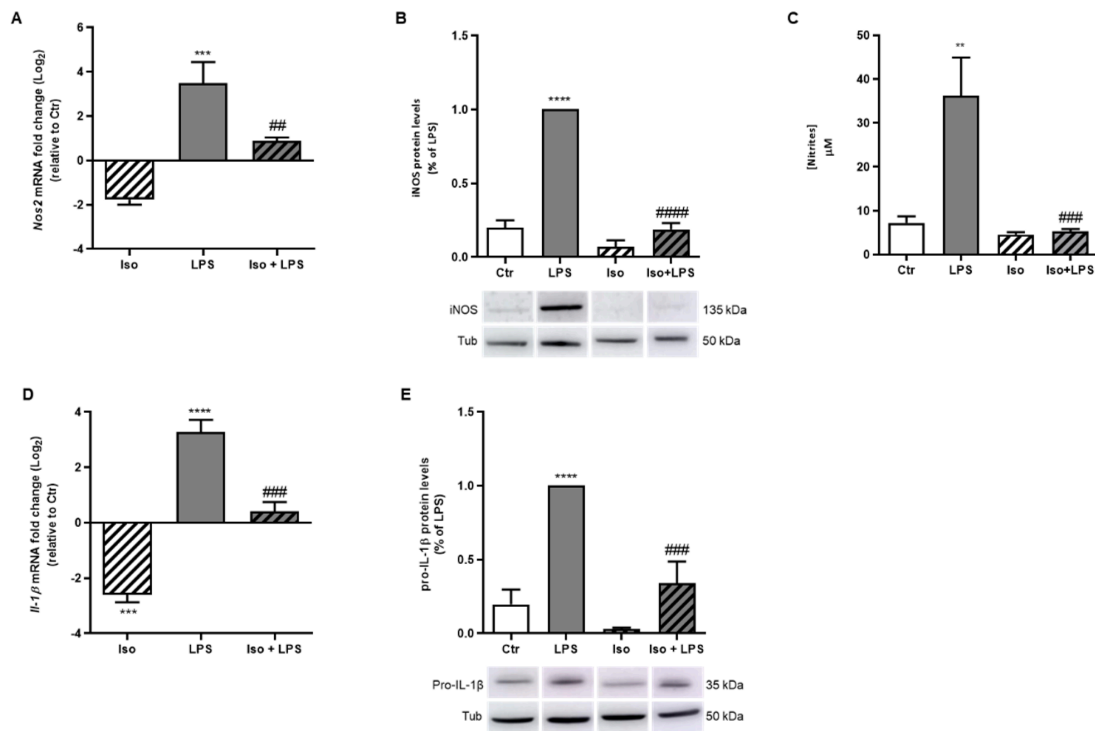
Fig. 5.Effect of Isoeugenol on inflammatory parameters in microglia cells exposed to LPS. BV-2 cells were exposed to Iso, in the presence or absence of LPS (50 ng/mL, 30 min after Iso incubation). *Nos2* and *Il-1β* mRNA levels were determined by real time RT-PCR, in BV2 cells exposed to Iso for 18 h (A, D). iNOS and pro–IL-1β protein levels were determined by WB, in BV2 cells exposed to Iso for 24 h (B, E). Representative blot images are presented. Nitric Oxide production was inferred by determining nitrites levels through Griess assay, in BV-2 cells exposed to Iso for 24 h (C). Values are the mean ± SEM of four to seven independent experiments and expressed relatively to control (Ctr) cells. Statistics: One-way ANOVA with Tukey's multiple comparisons test (*). $p < 0.05$ was considered significant. ** $p < 0.01$, *** $p < 0.001$ and **** $p < 0.0001$, compared Ctr cells (in A and D, Ctr=0 ($Log_2$1)); ## $p < 0.01$, ### $p < 0.001$ and #### $p < 0.0001$, compared LPS. Legend: Iso − Isoeugenol.

As expected, the *Toll-like* receptor agonist LPS induced a significant increase in *Nos2* (Fig. 5A) and *Il-1β* (Fig. 5D) gene expression, as well as in the levels of their encoded proteins, iNOS (Fig. 5B) and pro–IL-1β (Fig. 5E), respectively, which was reversed by Iso. Moreover, LPS–triggered nitrite production was also significantly decreased in microglia cells exposed to Iso (Fig. 5C). The overall results strongly indicate that Iso has a potent anti-inflammatory role in a neuroinflammation context.

3.6. Isoeugenol decreased the body weight of 6 mo treated animals and no alterations were detected in the fasting glucose and triglycerides

Taking into account the previous results, we further explored Iso effect in vivo, in AD mice with 5 months (early AD stage). Female mice were intranasally administered with Iso (50 mg/kg) for 30 days and sacrificed. To monitor animals' welfare, we first determined Iso-induced alterations in the body and adipose tissue weight, as well as in glucose and triglycerides levels (Fig. 6).
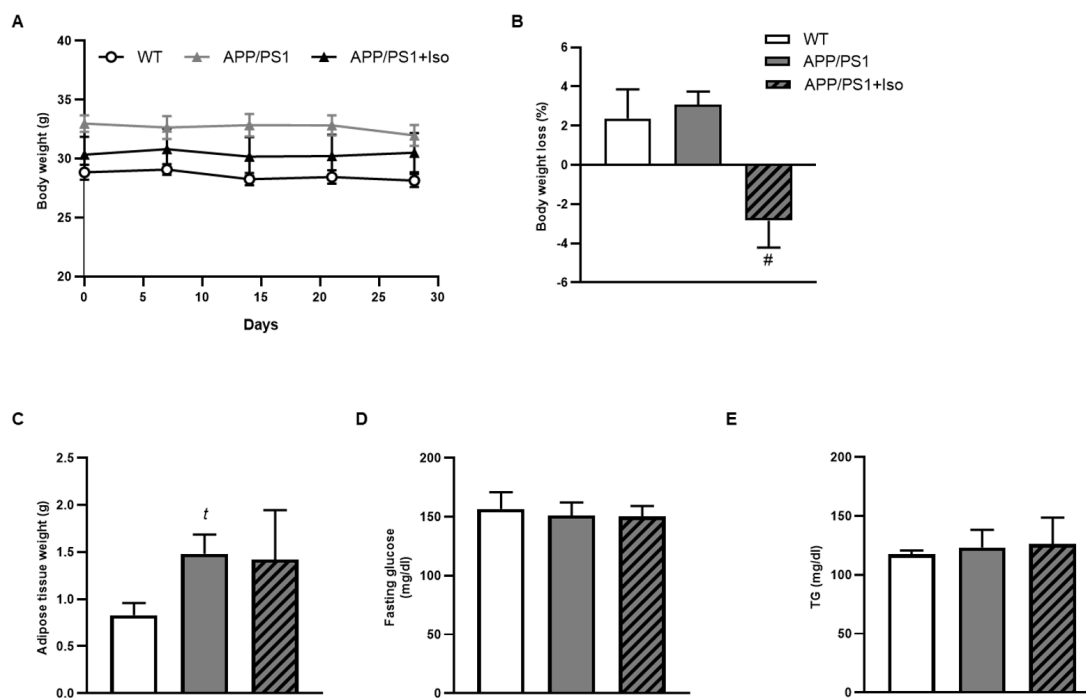
Fig. 6. Effect of Isoeugenol on demographic and metabolic parameters of 6 mo AD mice. Body weight (A), percentage of body weight loss (B), Adipose tissue weight (C), Fasting Glucose (D) and Triglycerides (E) were measured in 6 mo female mice, administered with Vehicle (PBS) or Iso (50 mg/kg; APP/PS1 only) for one month. Data correspond to the mean ± SEM of five to sixindependent experiments. Statistics: Unpaired t-test (t) and One-way ANOVA with Tukey's multiple comparisons test (#). $p < 0.05$ was considered significant. (t) $p < 0.05$, compared to WT and (#) $p < 0.05$, compared to APP/PS1. Legend: Iso − Isoeugenol; TG − Triglycerides; WT − wild-type.

This preliminary study showed that Iso induced a decrease in the body weight of APP/PS1 treated mice (APP/PS1+Iso compared to APP/PS1 animals; Fig. 6B) although it did not affect the weight of the adipose

tissue of AD mice, which increased, compared to the WT (Fig. 6C). However, no alterations were detected in the fasting glucose (Fig. 6D) and triglycerides (TG; Fig. 6E) values among groups.

3.7. Isoeugenol reduced brain Aβ peptides levels in mice with early AD progression

We further determined brain Aβ peptides levels and, as expected, APP/PS1 mice displayed increased $A\beta_{40}$ (Fig. 7A) and $A\beta_{42}$ (Fig. 7B) levels, compared to wild-type (WT).
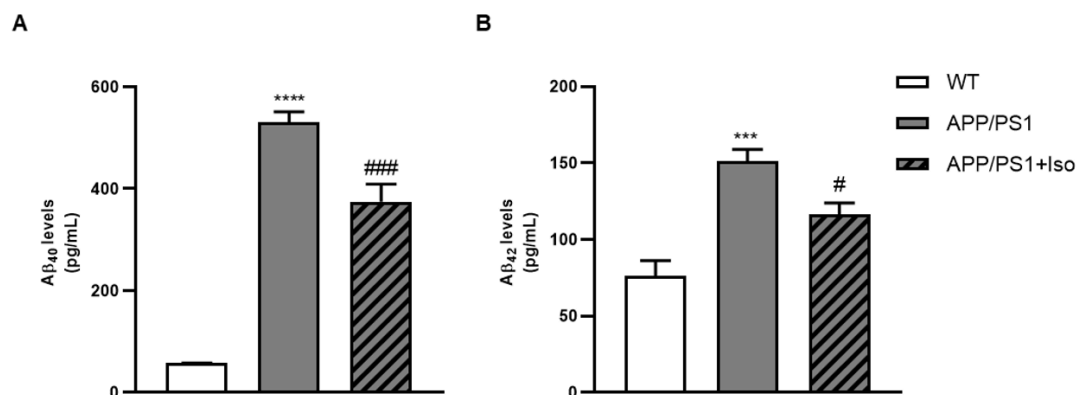

Fig. 7. Effect of Isoeugenol on Aβ peptides levels in the brain of 6 mo AD mice. $A\beta_{40}$ (A)and $A\beta_{42}$ levels (B)detected in the brain of WT and APP/PS1 6 mo female mice, administered with Vehicle (PBS) or Iso (50 mg/kg; APP/PS1 only) for one month. Data correspond to the mean ± SEM of five to sixindependent experiments. Statistics: One-way ANOVA with Tukey's multiple comparisons test. $p < 0.05$ was considered significant. *** $p < 0.001$ and **** $p < 0.0001$, compared to WT; # $p < 0.05$ and ### $p < 0.001$, compared to APP/PS1. Legend: Iso − Isoeugenol; WT − wild-type.

Of notice, Iso administration decreased both $A\beta_{40}$ and $A\beta_{42}$ in APP/PS1 mice (APP/PS1+Iso), compared to untreated AD mice (APP/PS1). In contrast, no differences were found in the plasma among APP/PS1 mice (either compared to WT or APP/PS1+Iso; data not shown).

We also evaluated locomotor activity and cognitive function of WT and APP/PS1 mice (Fig. 8) at this disease stage.
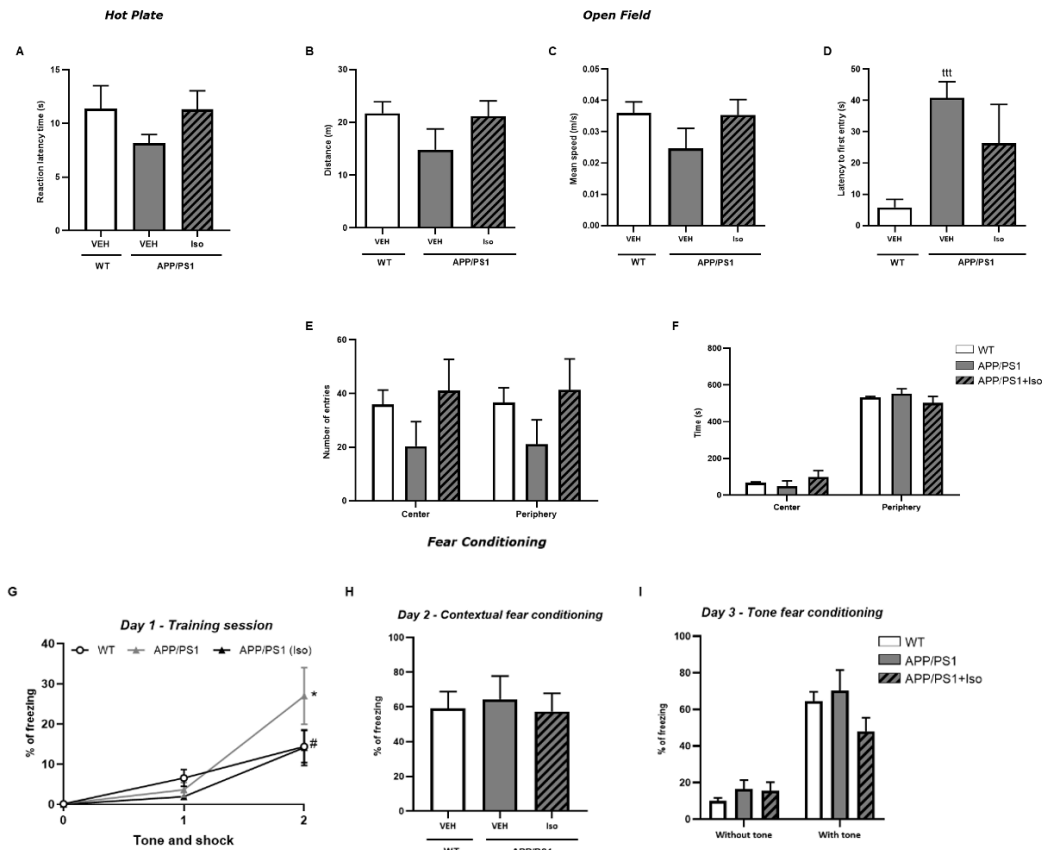
Fig. 8. Effect of Isoeugenol on locomotor activity and cognitive function of 6 mo AD mice. Hot plate (A), Open Field (B–F) and Fear Conditioning (G–I) behavioral tests performed with WT and APP/PS1 6 mo female mice, administered with Vehicle (PBS) or Iso (50 mg/kg; APP/PS1 only) for one month. Data correspond to the mean ± SEM of five to six independent experiments. Statistics: Unpaired t-test (t) and Two-way ANOVA (* and #) with Tukey's multiple comparisons test. $p < 0.05$ was considered significant. * $p < 0.05$ and (ttt) $p < 0.001$, compared to WT; # $p < 0.05$, compared to APP/PS1. Legend: Iso − Isoeugenol; WT − wild-type.

According to our results, APP/PS1 untreated animals showed increased anxious behavior compared to WT, only inferred by the time spent to make the first entry in the central zone of the open field arena. The animals treated with Iso (APP/PS1+Iso) apparently are less anxious, although APP/PS1+Iso data towards a reduction in latency time to enter in the central arena are not significantly different from that observed with untreated mice (APP/PS1) and it also lacks statistical significance when compared to WT (Fig. 8D). The data also reflects that all animal groups have equivalent locomotor activity. Moreover, % of total freezing in the training session for the contextual fear conditioning test, has shown increased fear

acquisition in diseased animals (APP/PS1, compared to WT) that was reduced by Iso treatment (APP/PS1+Iso vs APP/PS1) (Fig. 8G).

3.8. Intranasal administration of Isoeugenol is safe for mice

Since no major phenotypic changes were detected at 6 mo, we further studied Iso intranasal administration at a higher concentration (100 mg/kg) in older animals (10-11 mo). Hence, we first performed pharmacokinetic studies and determined demographic and biochemical variations as well as histological alterations in WT animals with the same genetic background as APP/PS1 transgenic mice, administered with the vehicle (VHE, PBS) or Iso.

3.8.1. Pharmacokinetic studies

The concentration-time profiles of Iso in plasma, brain and lung of WT mice after intranasal administration (100 mg/kg, single dose) are presented in Fig. 9, while pharmacokinetic parameters are shown in Table I.
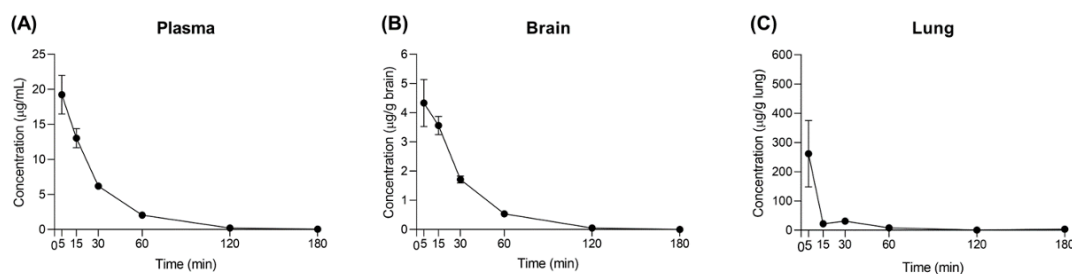

Fig. 9. Pharmacokinetic studies. Concentration-time profile in biological matrices of plasma (A), brain (B) and lung (C) of WT mice, after 5, 15, 30, 60, 120 and 180 min of Iso intranasal administration (100 mg/kg). Symbols correspond to mean values ± SEM (n = 4).

Pharmacokinetic parameters [a]	Plasma	Brain	Lung
t_{max} (min)	5.00	5.00	5.00
C_{max} (µg/mL)	26.41	4.34[b]	348.16[b]
AUC_t (µg min/mL)	599.05	140.87[c]	4030.85[c]
AUC_{inf} (µg min/mL)	604.28	142.15[c]	4091.75[c]
AUC_{extrap} (%)	0.86	0.90	1.49
k_{el} (min^{-1})	0.038	0.039	0.022
$t_{1/2\beta}$ (min)	18.12	17.65	31.27
AUC_t ratios			
$AUC_{brain/plasma}$	0.23	-	-
$AUC_{lung/plasma}$	6.73	-	-

Table I – Pharmacokinetic parameters of Isoeugenol in mouse plasma, brain and lung after intranasal administration (100 mg/kg).

a. Parameters estimated using mean concentration-time profiles obtained from 4 mice per time point (n = 4).

b. Values expressed in µg/g;

c. Values expressed in µg.min/g.

AUC_{extrap} – extrapolated area under the concentration-time curve; AUC_{inf} – area under the concentration-time curve from time zero to infinity; AUC_t – area under the concentration-time curve from time zero to the time of last measurable concentration; C_{max} – maximum concentration; k_{el} – elimination rate constant; $t_{1/2\beta}$, apparent elimination half-life; t_{max}, time required to reach the maximum concentration.

Considering AUC_{extrap} values (< 20%) in plasma, brain and lung, it was confirmed that the number of analyzed samples was adequate for a reliable calculation of K_{el}, AUC_t and AUC_{inf} values (Table I).

Accordingly, Iso was absorbed quickly (t_{max} = 5 min in plasma) and removed from the blood due to either a fast distribution into peripheral tissues (t_{max} = 5 min in brain and lungs) or elimination ($t_{1/2\beta}$ = 18.12) (Table I). These results are in agreement with those observed by others, after intravenous and oral administration of Iso (Badger et al, 2002; Hong et al, 2013). Although Iso levels in the brain and lung were not determined by Hong et al. (2013), the authors suggested that the molecule might display a fast

distribution to tissues due to its low alpha half-life distribution time (7-10 min) and steady-state apparent volume of distribution (11-25.2 L/kg) after intravenous dosing, which exceeds total body water volume (0.6 L/kg) and indicates extensive distribution to extravascular tissues. Iso fast distribution might also be related to its low molecular weight (164.2 g/mol) and lipophilicity (octanol-water partition coefficient (logP) = 3.04), allowing it to quickly spread across cell membranes. On the other hand, its fast elimination may be due to Iso facilitated conversion into phase II metabolites (Badger, 2002), hence promoting its excretion as glucuronide or sulphate derivatives.

Considering the doses of Iso administered by Hong et al. (2013) to mice by intravenous (35 mg/kg) and oral routes (35, 70 e 140 mg/kg), AUC values in plasma were dose-normalized, in order to compare with AUC_{inf} and AUC_t values of the present study (100 mg/kg) after intranasal administration. The dose-normalized AUC_{inf} value after intranasal administration (6.04 μg min/mL/kg) was similar to that observed after intravenous administration (6.76 μg min/mL/kg) (Hong et al, 2013). In contrast, dose-normalized AUC_t values (1,91, 1,68, 1,45 μg min/mL/kg) after oral administration (Hong et al, 2013) were lower than those of the present study (5.99 μg min/mL/kg), suggesting that the systemic exposure of Iso after intranasal and intravenous administration routes are identical, and both are superior to the oral route.

Regarding tissue exposure, differences were observed between the three biological matrices herein analyzed (plasma, brain and lung; Table I). Accordingly, the brain and lung displayed the lowest and the highest AUC_t values, respectively. Indeed, also C_{max} values and lung-plasma ratios were much higher than in the other matrices, suggesting direct passage of Iso to the lungs, when administered intranasally. Although $t_{1/2\beta}$ values were short for all matrices, $t_{1/2\beta}$ was higher in lung (31.27 min vs. 18.12 e 17,65 min; Table I), suggesting that Iso elimination from the lung is slower compared to the plasma and the brain. For this reason, histopathological analysis of lung, and other organs, were performed.

3.8.2. Metabolic, biochemical and histological data

To study the metabolic impact of Iso upon intranasal administration on mice, glucose and lipid metabolism were analyzed in 11 mo WT females mice serum (Fig. 10A-E). We further evaluated if Iso administration was safe for mice liver and kidney. Accordingly, we examined the serum levels of liver parameters, namely GOT, GGT, and ALP (Fig.10F-H), and of kidney parameters, particularly albumin, creatinine, and urea levels (Fig. 10I-K).
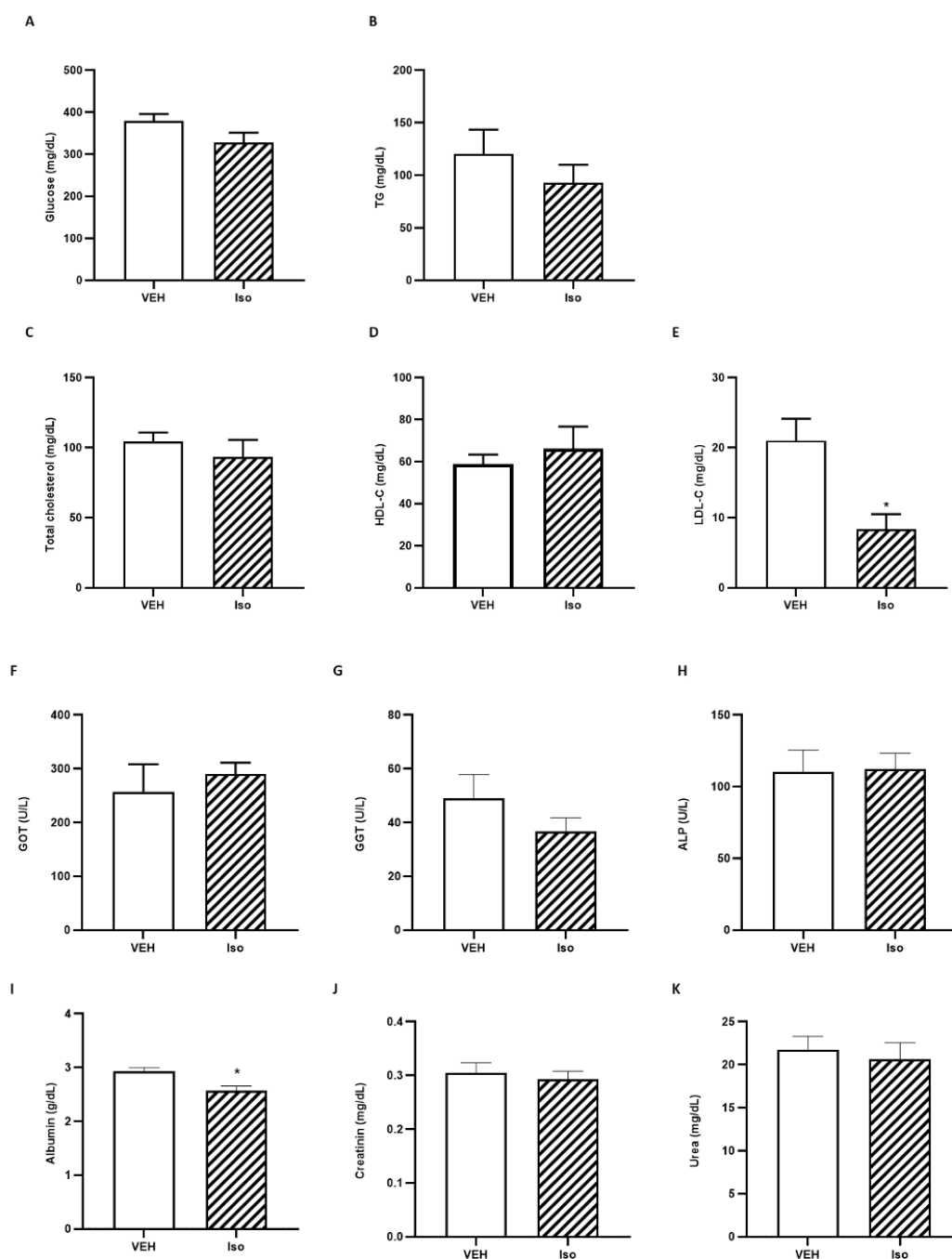
Fig. 10. Iso effect on 11 mo WT female's metabolic and biochemical parameters. 11 mo female mice, were administered with Vehicle (PBS) or Iso (100 mg/Kg) for one month. The metabolic parameters glucose (A), triglycerides (TG; B), total cholesterol (C), high-density lipoprotein cholesterol (HDL-C; D) and low-density lipoprotein cholesterol (LDL-C; E); the markers of liver function glutamic-oxaloacetic transaminase (GOT; F), gamma-glutamyl transferase (GGT; G), and alkaline phosphatase (ALP; H), and of kidney function albumin (I), creatinine (J), and urea (K) were determined. Data correspond to the mean ± SEM of five to sixindependent

experiments. Statistics: Unpaired t-test. $p < 0.05$ was considered significant. * $p < 0.05$, compared to VEH.

Legend: Iso – Isoeugenol; WT – wild-type.

As shown in Fig. 10 (A-E), no alterations in glucose (Fig. 10A), triglycerides (TG; Fig.10B), and total cholesterol (Fig. 10C) levels were detected in 11-mo animals after Iso administration, compared to mice administrated with PBS (Vehicle - VEH). Interestingly, Iso significantly reduced LDL cholesterol (Fig. 10E) when compared to the VEH group. These results suggest that Iso is absent of deleterious metabolic effects, and its intranasal administration might have a positive impact on cholesterol metabolism.

Moreover, and according to data depicted in Fig 10 (I-K) none of the parameters analyzed were affected by Iso administration (compared to VEH) except albumin, which was slightly decreased by Iso. However, in mice, the normal range for albumin concentration in the blood is typically between 2.5 to 3.5 g/dL, so the values obtained are within physiological levels.

In addition, potential renal, lung, brain, heart, and liver damage were also assessed in hematoxylin- and eosin-stained sections of each organ by microscopy (Fig. 11).
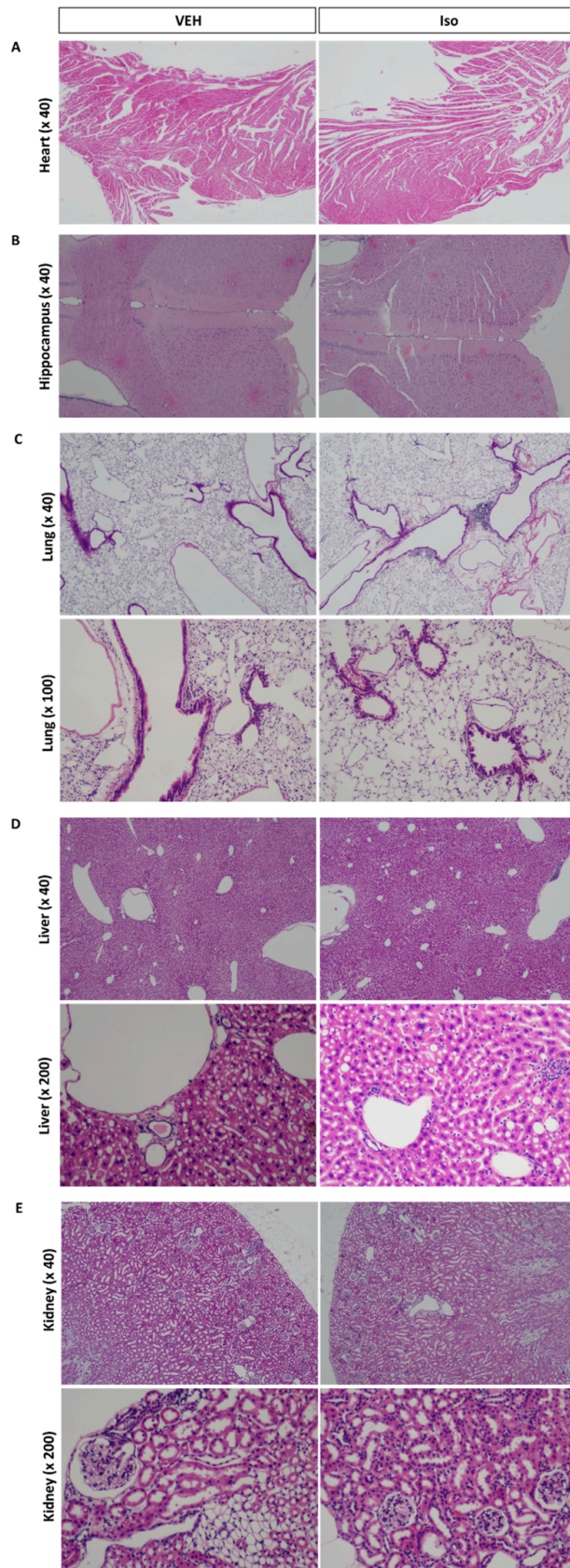
Figure 11. 11 mo WT females' histopathology analysis. Histopathology of the heart (A), brain (B), lung (C), liver (D) and kidney (E) of 11 mo female WT mice intranasally administered with Vehicle (PBS) or Iso (100 mg/Kg) for one month. Representative images of each organ sections stained with hematoxylin and eosin at 40×, 100×, or 200× magnification.

No negative histopathological changes in the heart (Fig. 11A) were found in Iso-treated mice relative to the VEH group. Indeed, we specifically assessed the interventricular septum as the anatomical structure controlling the transmission of the action potential between the atria and ventricles to exclude any pro-arrhythmic potential. Increased cell activation in the brain was verified after intranasal administration of Iso, as depicted in Fig. 11B. In the lung slices of Iso-treated mice, some infiltration of lymphocytes and bronchiolar hyperplasia was detected (Fig. 11C), although the latter was also observed in some animals in the VEH group. Histopathological analysis of the liver slides showed hepatic steatosis in the control animals (Fig. 11D), revealing a pattern of histopathological alterations in the livers of these animals, which was also maintained in Iso-treated mice. Cellular eosinophilia and tubular epithelial hypertrophy were observed in the kidneys of the Iso-treated animals (Fig. 11E). Of notice, some adverse renal and liver reactions have been also reported for dimethyl fumarate (EMA, 2023), a drug approved for the treatment of multiple sclerosis, which also belongs to the class of skin allergens that behave like Michael acceptors. Additional in vivo studies with lower doses of Iso should be conducted to verify the maintenance of drug efficacy with potential mitigation of the related histopathological alterations.

To assure animal well-being, the body weight of WT and APP/PS1 male mice was measured every week during Iso intranasal administration period (one month) (Fig. 10A and B). Adipose tissue weight (Fig. 10C), Brain tissue weight (Fig. 10D), and the metabolic parameters, namely glucose levels, determined during the intraperitoneal Glucose Tolerance Test (GTT; Fig. 12E and F) and after 6 h fast (Fasting Glucose; Fig. 12G), and triglycerides (Fig. TG; 12H) were also measured.
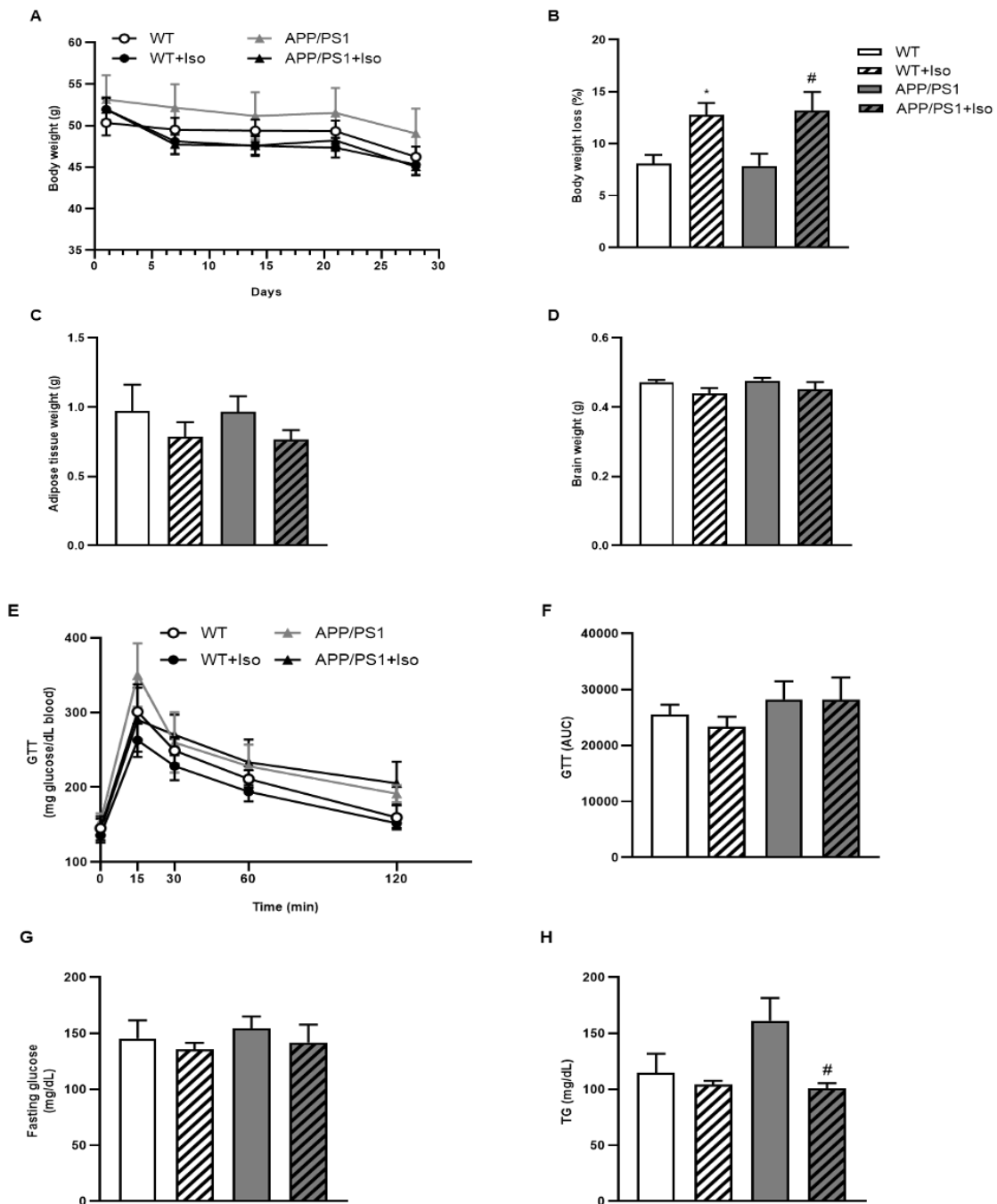
Figure 12. Effect of Isoeugenol on biochemical parameters of 11 mo AD mice. Body weight (A), percentage of body weight loss (B), Adipose tissue weight (C), Brain tissue weight (D), Glucose levels (E–G) and Triglycerides (E) were measured in 11 mo male mice, administered with Vehicle (PBS) or Iso (100 mg/Kg; APP/PS1 only) for one month. Data correspond to the mean ± SEM of five to sixto eightindependent experiments. Statistics: One–way ANOVA with Tukey's multiple comparisons test. p < 0.05 was considered significant. * p < 0.05,

compared to WT and (#) p < 0.05, compared to APP/PS1. Legend: Iso − Isoeugenol; GTT − Glucose Tolerance Test; AUC − Area Under the Curve; TG − Triglycerides; WT − wild-type.

As observed in Fig. 12, there are no differences between WT and APP/PS1 animals weight administered with VEH alone (Fig. 12A and B). However, both groups were equally affected by Iso, which induced a significant weight loss in WT and APP/PS1-treated mice, compared to untreated animals, although it did not compromise animal well-being since it was less than 15%. Moreover, no differences were observed in organs weight (i.e., adipose tissue and brain; Fig. 12C and D) and in glucose blood levels (fasting and determined by the Glucose Tolerance Test; Fig.E-G). In contrast, a significant decrease in triglycerides (TG) was detected in Iso-treated APP/PS1 mice, compared to the group administered with PBS (VEH) (Fig. 12H)

3.9. Isoeugenol reduces Aβ peptides levels in the cortex and plasma of mice with late AD progression

We next evaluated Aβ peptides levels in the cortex, hippocampus and plasma of WT and APP/PS1 treated with PBS (VEH) or Iso (Fig. 12).
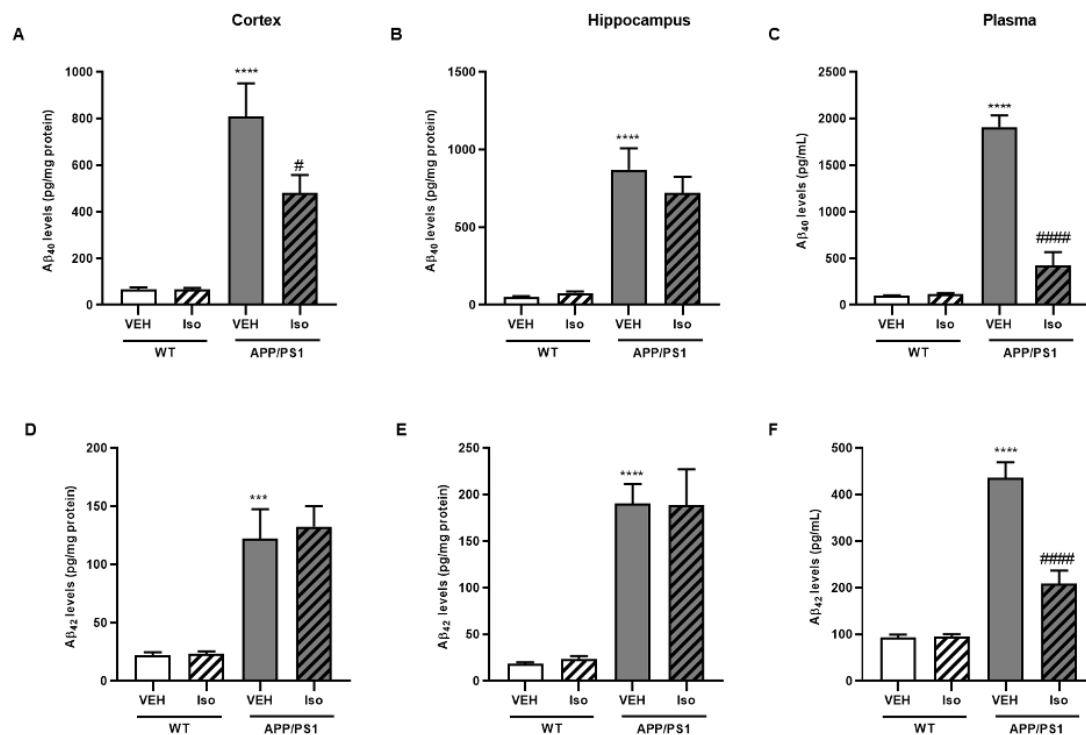
Fig. 12. Effect of Isoeugenol on Aβ peptides levels in the cortex, hippocampus, and plasma of 11 mo AD mice. $A\beta_{40}$ and $A\beta_{42}$ levels detected in the cortex (A, D), hippocampus (B, E) and plasma (C, F) of WT and APP/PS1 11 mo male mice, administered with Iso (100 mg/kg) for one month. The results represent the mean ± SEM of three to eight animals. Statistics: One-way ANOVA with Tukey's multiple comparisons test. $p < 0.05$ was considered significant. *** $p < 0.001$ and **** $p < 0.0001$, compared to WT VEH; # $p < 0.05$ and #### $p < 0.0001$, compared to APP/PS1 VEH. Legend: Iso – Isoeugenol; VEH – Vehicle; WT – wild-type.

As expected, $A\beta_{40}$ (Fig. 10A-C) and $A\beta_{42}$ (Fig. 10D-F) peptides levels are significantly higher in the cortex, hippocampus and plasma of APP/PS1 mice compared to WT. However, Iso treatment only decreased $A\beta_{40}$ levels in the cortex (Fig. 10A) and both $A\beta_{40}$ and $A\beta_{42}$ levels in the plasma (Figs. 10C and 10F, respectively), with no alterations observed in the hippocampus (Figs. 10B and 10E).

3.10. Isoeugenol modulates the transcriptional signature of APP/PS1 mice hippocampus: increase in Hmox1, Iba1, Ppargc1α and Bdnf

We further examined Iso-induced alterations in genes related with the amyloidogenic pathway (i.e., *hAPP* and *Bace1*), the antioxidant cell defense (i.e., *Hmox1*), the inflammatory pathway (i.e., Interleukin 1β, *Il-1β*), Aβ production (i.e., Protein kinase C gamma, *Prkcg*), microglia function (i.e., Ionized calcium binding

adaptor molecule 1, *Iba1* and Triggering receptor expressed on myeloid cells 2, *Trem2*), energy metabolism (i.e., Peroxisome proliferator–activated receptor gamma coactivator 1–alpha, *Ppargc1α*), and neuroprotection (i.e., Brain–derived neurotrophic factor, *Bdnf*), in WT and APP/PS1 cortex and hippocampus (Fig. 13).
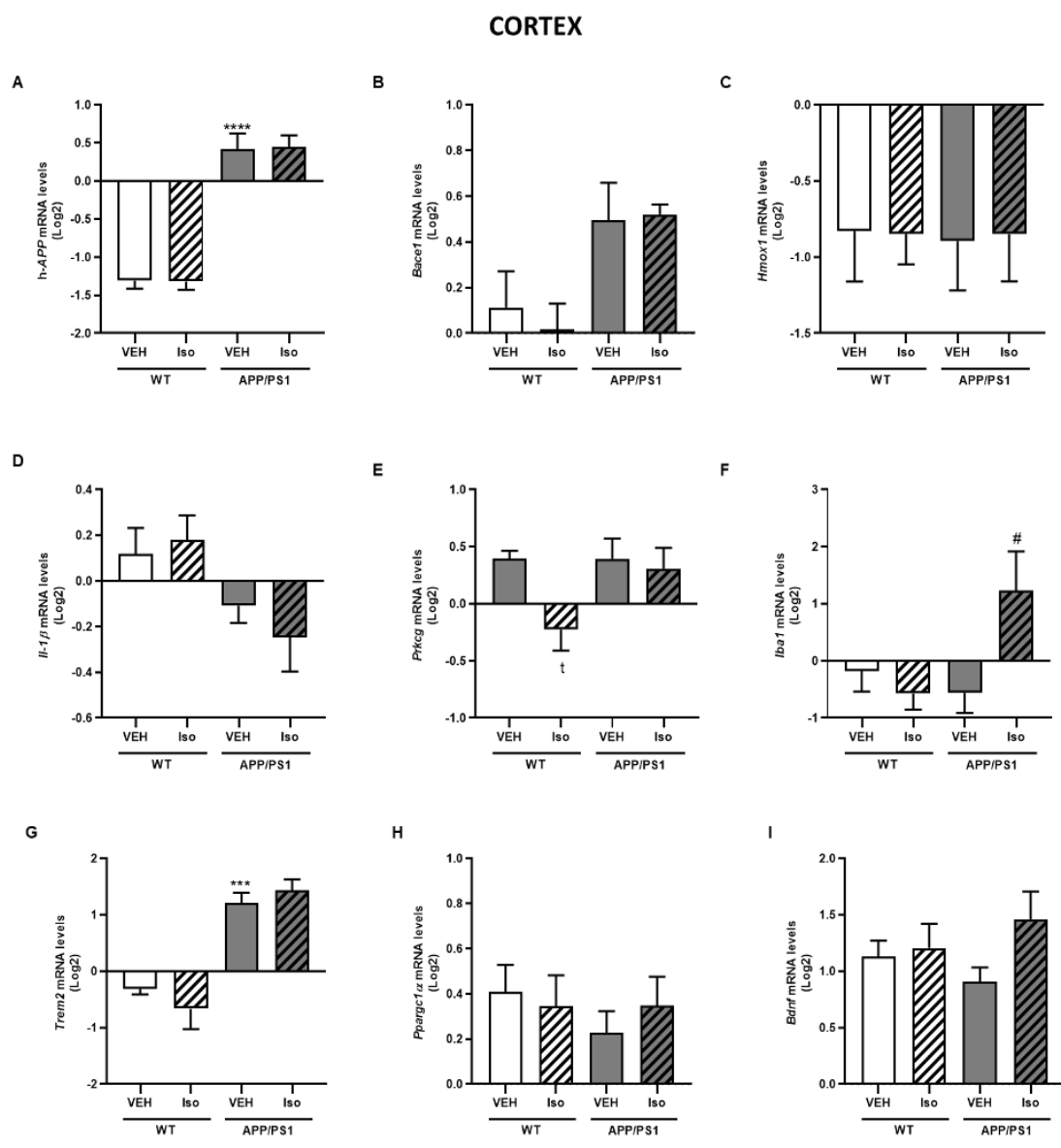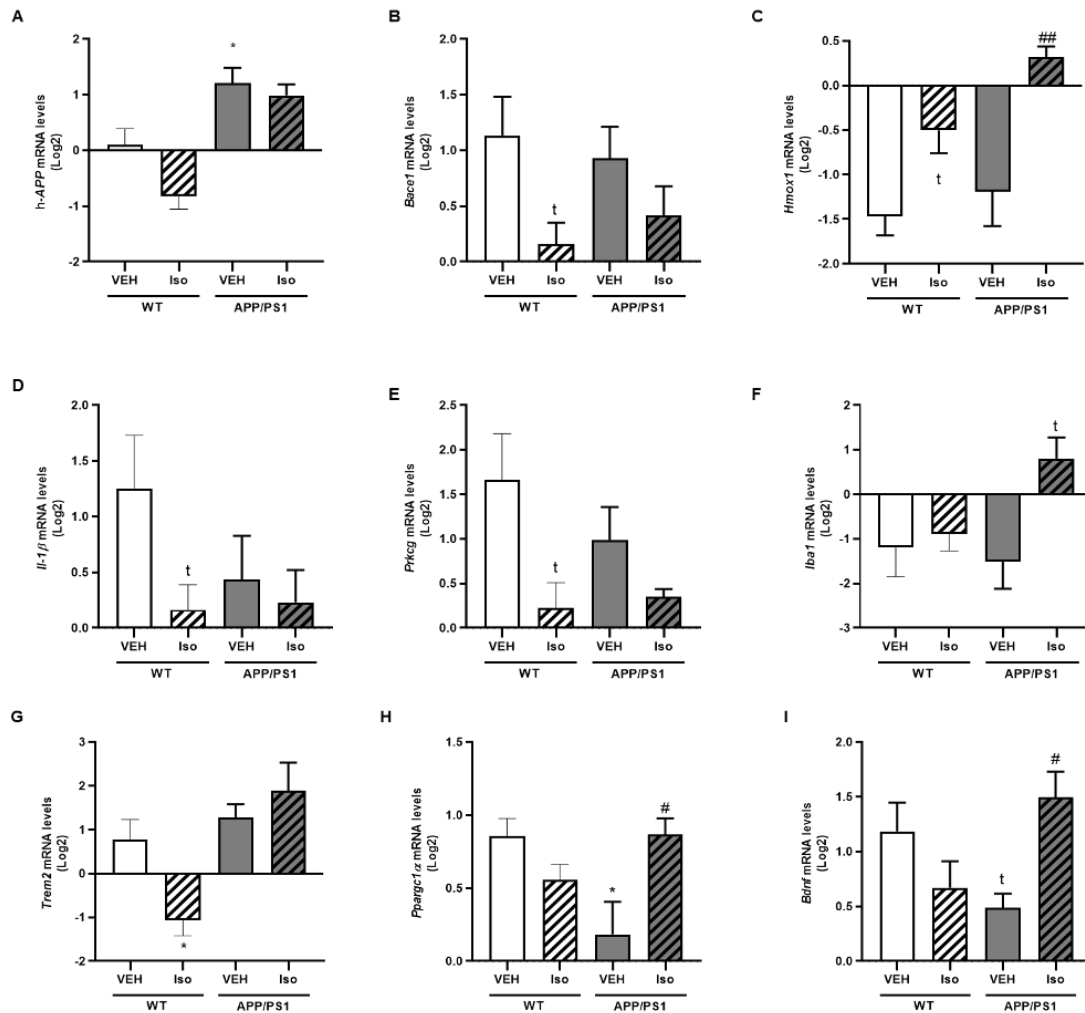
Fig. 13. Iso-induced gene expression alterations in the cortex and hippocampus of WT and AD mice. The mRNA l*evels* of the genes *hAPP* (A), *Bace1* (B), *Hmox1* (C), *Il-1β* (D), *Prkcg* (E), *Iba1* (F), *Trem2 (G)*, *Ppargc1α (H)* and *Bdnf* (I) were determined in the Cortex and Hippocampus of 11 mo WT and APP/PS1 male mice, intranasally administered with Iso (100 mg/kg) or PBS (VEH), for one month. The results represent the mean ± SEM of four to six animals. Statistics: Unpaired t-test (t) and one-way ANOVA with Tukey's multiple comparisons test (* and #). $p < 0.05$ was considered significant. (t) $p < 0.05$, compared to the VEH of the respective group; * $p < 0.05$, ***$p < 0.001$ and **** $p < 0.0001$, compared to WT VEH; # $p < 0.05$ and ## $p < 0.01$, compared to APP/PS1 VEH. Legend: Iso – Isoeugenol; VEH – Vehicle; WT – wild-type.

According to Fig.13, the *h-APP* gene expression was significantly augmented in both the cortex (Fig. 13A, CORTEX upper panel) and the hippocampus (Fig. 13A, HIPPOCAMPUS lower panel) of APP/PS1 transgenic

animals (compared to WT), which was anticipated in this AD mice model. The *hAPP* gene overexpression was not affected by Iso-treatment. With exception of increased *Trem2* expression in the cortex of APP/PS1 mice (Fig. 13D, CORTEX upper panel), no other significant differences in gene expression were detected in the cortex of transgenic animals, compared to WT. Nevertheless, *Prkcg* and *Iba1* expression was induced by Iso, in WT and APP/PS1 mice, respectively (Fig. 13E and F, CORTEX upper panel).

Phenotypic-related alterations in the expression of *Ppargc1α* and *Bdnf* were detected in the hippocampus (Fig. 13H and I, HIPPOCAMPUS lower panel, respectively). Both gene expression levels were reduced in transgenic mice (APP/PS1 VEH, compared to WT VEH), which were reverted in Iso-treated APP/PS1 mice (APP/PS1+Iso *vs* APP/PS1). Moreover, Iso also modulated the mRNA levels of the other genes studied by inducing a decrease in *Bace1*, *Il-1β*, *Prkcg* and *Trem2*, in WT animals (Fig. 13B, D, E and G, HIPPOCAMPUS lower panel, respectively), and an increase in *Hmox1*, in both WT and APP/PS1 mice, and in *Iba1*, in APP/PS1 only (Fig. 13C and F, HIPPOCAMPUS lower panel, respectively).

3.11. APP/PS1 mice does not display differences regarding locomotor activity or pain sensitivity

The effect of Iso on pain sensitivity and on locomotor activity of WT and APP/PS1 mice was evaluated through the hot plate test and the open field test, respectively (Fig. 14).
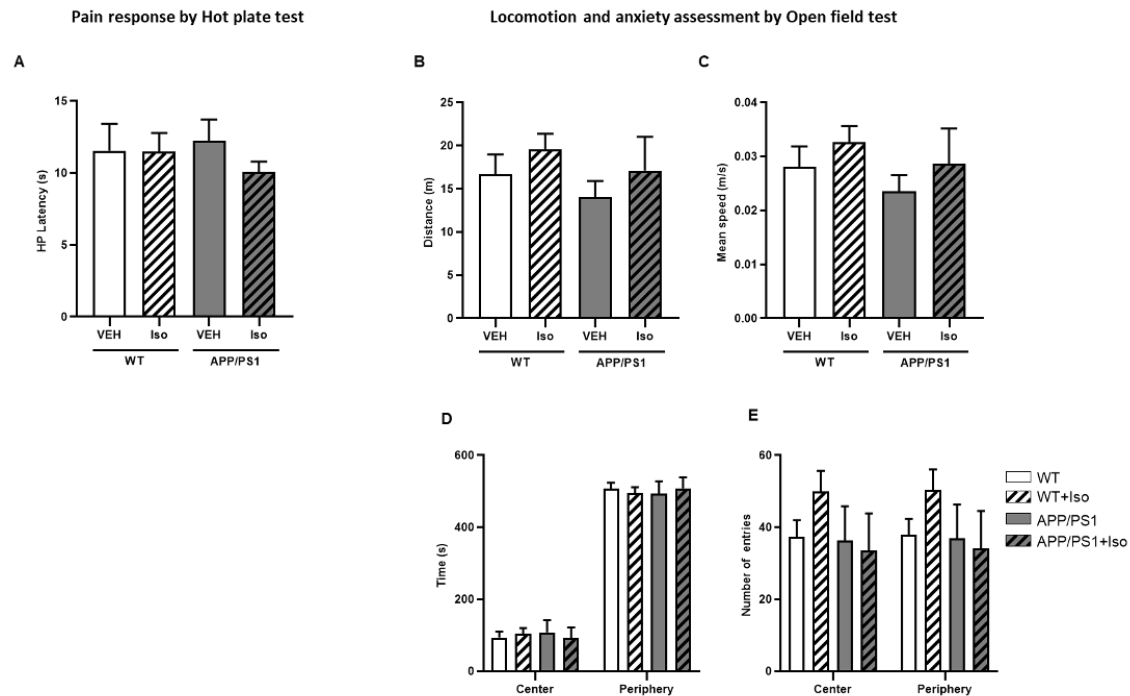
Fig. 14. Effect of Isoeugenol on pain sensitivity and locomotor activity in WT and APP/PS1 mice. 11 mo male mice intranasally administrated with VEH or 100 mg/kg Iso for one month were evaluated for pain sensitivity and locomotor activity using the hot plate (A) and the open field (B-E) tests, respectively. The results represent the mean ± SEM of six to eight animals. Legend: Iso − Isoeugenol; VEH − Vehicle; WT − wild-type.

The results showed that there were no differences in response latency to a thermal stimulus between all animal groups (Fig. 14A), suggesting that WT and APP/PS1 mice have similar pain sensitivity, which was not affected by Iso. Moreover, no significant differences were detected between groups in the total distance travelled (Fig. 14B) and in the mean speed (Fig. 14C), demonstrating that the animals were equivalent in terms of locomotion. On the other hand, there were no differences in the time spent and number of entries in the central or peripheral zones (Fig. 14D, E), reflecting no compromise by the disease at this stage and/or by Iso intranasal administration of the animal´s natural exploratory behavior.

3.12. Intranasal administration of Iso does not affect the anxiety levels of APP/PS1 mice

Iso effect on mice anxiety levels were evaluated by the elevated plus−maze test (Fig. 15).

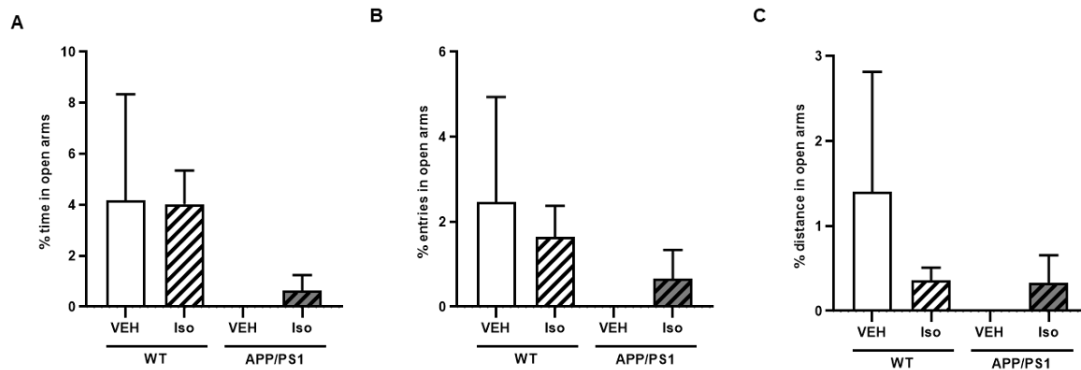**Anxiety assessment by Elevated Plus Maze test**

Fig. 15. Effect of Isoeugenol on anxiety levels in WT and APP/PS1 mice. 11 mo male mice intranasally administrated with VEH or 100 mg/kg Iso for one month were evaluated for anxiety using the elevated plus-maze(A-C)test. The results represent the mean ± SEM of six to eight animals. Legend: Iso – Isoeugenol; VEH – Vehicle; WT – wild-type.

According to the results, there are no differences between all groups, as determined by the time spent (Fig. 15A), the number of entries (Fig. 15B) and the distance travelled in the open arm (Fig. 15C), suggesting that both WT and APP/PS1 11 mo animal have similar anxiety levels, which are not affected by Iso treatment.

3.13. Intranasal administration of Iso improves memory deficits in APP/PS1 mice

The effect of Iso on WT and APP/PS1 mice memory was also evaluated, namely the spatial memory (using the Y-maze test; Fig. 16A-C) and the social recognition memory (through the novel object recognition test; Fig. 16D, E).
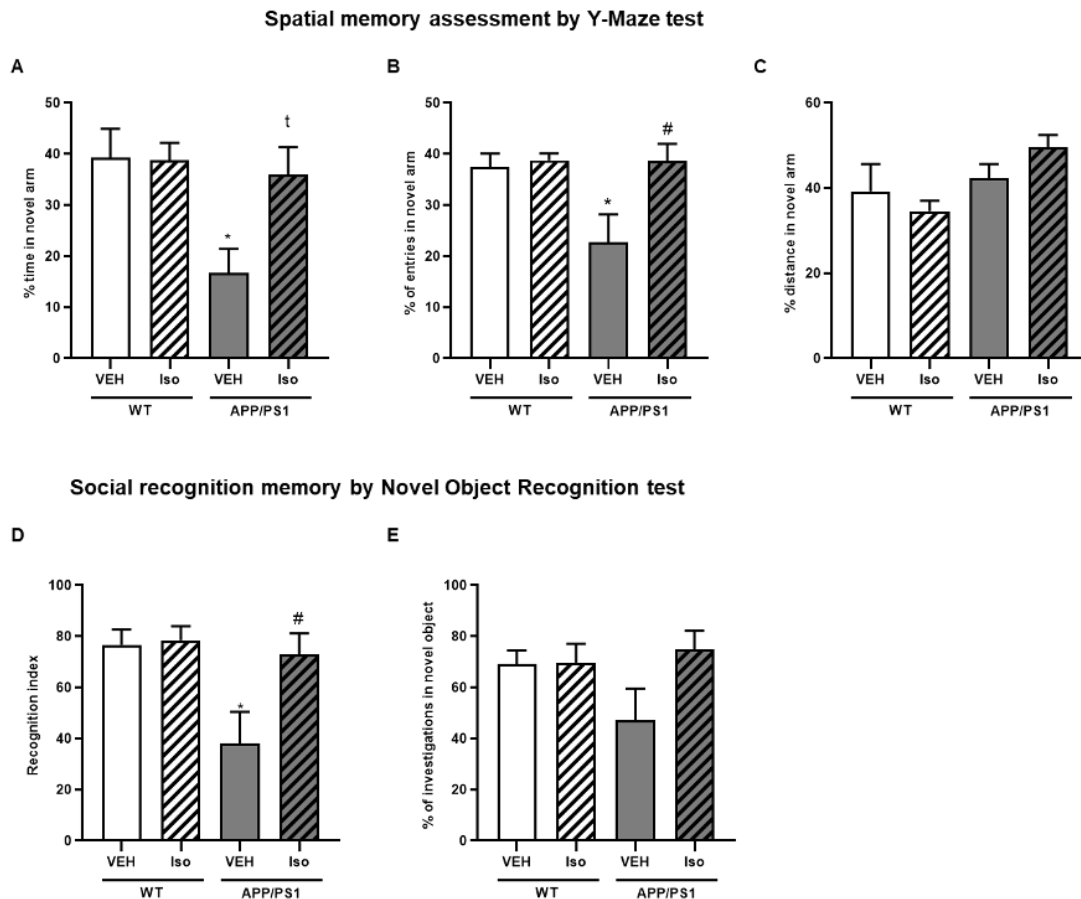
Spatial memory assessment by Y-Maze test

Social recognition memory by Novel Object Recognition test

Fig. 16.Effect of Isoeugenol on WT and APP/PS1 spatial and social recognition memory. 11 mo male mice intranasally administrated with VEH or 100 mg/kg Iso for one month were evaluated for spatial memory using the Y-maze (A–C) test and for social recognition memory using the novel object recognition (D–E) test. The results represent the mean ± SEM of four to seven animals. Statistics: Unpaired t-test (t) and one-way ANOVA with Tukey's multiple comparisons test (* and #). $p < 0.05$ was considered significant. * $p < 0.05$, compared to WT VEH; (t) and (#) $p < 0.05$, compared to APP/PS1 VEH. Legend: Iso − Isoeugenol; VEH − Vehicle; WT − wild-type.

The results demonstrated that VEH–treated APP/PS1 mice entered and spent less time in the novel arm (compared to VEH–exposed WT mice), which was reverted by Iso (APP/PS1 Iso vs APP/PS1 VEH; Fig16A and B). Moreover, the recognition index of the VEH–treated APP/PS1 mice was significantly lower than that of the VEH–exposed WT mice, which was also reverted in mice administered with Iso (Fig. 16D). Overall, these results indicate that both spatial and non-emotional memory is impaired in the transgenic AD mouse model and both were significantly improved by Iso treatment.

We also evaluated the hippocampal–dependent long–term contextual/associative memory, which was assessed by the Fear Conditioning test (Fig. 17).
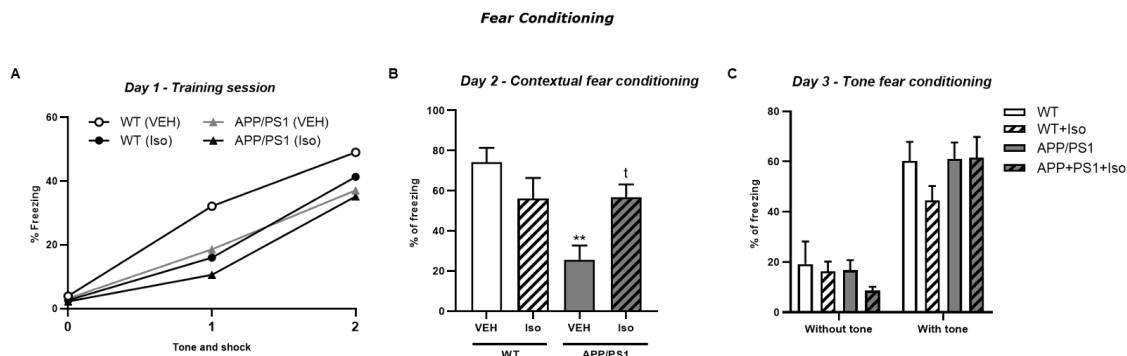

Fig. 17.Effect of Isoeugenol on WT and APP/PS1 hippocampal–dependent long–term contextual/associativememory. 11 mo male mice intranasally administrated with VEH or 100 mg/kg Iso for one month were evaluated for hippocampal–dependent long–term contextual/associative memory using the Fear Conditioning test (A–C). The results represent the mean ± SEM of five to six animals. Statistics: Unpaired t–test (t) and one–way ANOVA with Tukey's multiple comparisons test (*). $p < 0.05$ was considered significant. (*) and (t) $p < 0.05$, compared to WT VEH and APP/PS1 VEH, respectively. Legend: Iso – Isoeugenol; VEH – Vehicle; WT – wild–type.

According to Fig. 17, all animals equally acquired fear, but Iso improved APP/PS1 mice contextual memory, since it reverted the % of animals' freezing, which was significantly reduced, compared to the WT VHE (Fig. 17B).

4. Discussion

The research data gathered from diverse neurodegenerative disease models (e.g., AD) in the last decade, strongly supports that Nrf2 activation, in the brain, mainly resulting from the inhibition of Keap1, might exert a disease–modifying positive outcome, in the context of neuroinflammation and neurodegeneration, proteostasis, as well as energy metabolism. Nevertheless, the molecules that activate Nrf2 do not act at the level of disease etiology. Instead, Nrf2 activators improve homeostasis, by promoting proteostasis and a favorable metabolic, antioxidant and anti–inflammatory cell environment, contributing to attenuate disease progression. In fact, excellent results have been obtained with a panoply of small molecules that activate Nrf2, in neurodegenerative disease models. These Nrf2 activators are

electrophilic molecules that react with Keap1 cysteine residues, hindering Keap1 of presenting Nrf2 for ubiquitination, hence leading to an undissociated Nrf2-Keap1 complex. As a result, newly synthetized Nrf2 is not degraded by the proteosome and translocate to the nucleus where it initiates the transcription of its target genes. Nevertheless, molecules able to cross the blood-brain barrier, with good pharmacokinetic and pharmacodynamic profile, need to be identified (Cuadrado et al, 2022).

In AD, Nrf2 detoxifying and antioxidant pathway was shown to be defective (Fão et al, 2019; Ramsey et al, 2007), which might underly the exacerbated oxidative stress, Aβ aggregates and neuroinflammation (all relevant hallmarks of this disease). Therefore, herein we proposed to evaluate the therapeutic potential of Isoeugenol (a skin allergen with electrophilic properties), in reverting some AD hallmarks, via Nrf2 activation. Accordingly, low molecular weight skin allergens, like Iso and dimethyl fumarate, are small molecules able to modify the sulfhydryl groups of Keap1's cysteine residues. This study was conducted in vitro (in mice microglia cells challenged with LPS and neuronal cells overexpressing the human APP with Swedish mutation, N2a-APPswe) and in vivo (in the AD double transgenic mice, APP/PS1). Therefore, in a first approach we confirmed Nrf2 activation by Iso, as inferred by the increased nuclear levels of Nrf2 protein and by quantification of Nrf2 activation (using a colorimetric kit), in nuclear extracts of N2a-APPswe cells exposed to Iso for 6 h (compared to untreated cells). However, Nrf2 might also be activated through the PI3K-AKT-GSK3β signaling pathway, which also has significant roles in cellular processes, such as metabolism, cell survival and proliferation, synapse formation, cytoskeleton organization and glucose transport (Gabbouj et al, 2019; Zhang et al, 2014). AKT activation (due to phosphorylation by PI3K), is well-known to further inactivate GSK3β (a pro-apoptotic protein kinase involved in Nrf2 cytoplasmatic sequestration and proteasomal degradation) through phosphorylation of GSK3β serine 9 residues, allowing Nrf2 translocation to the nucleus (Ali et al, 2018; Ambacher et al, 2012; Cuadrado et al, 2018). Therefore, besides Nrf2 activation, we also evaluated AKT activation and GSK3β inactivation induced by Iso, in N2a-APPswe cells. Both AKT and GSK3β phosphorylated levels were decreased in N2a-APPswe cells (compared to N2a-wt), which might partially explain the sustained Nrf2 cytoplasmatic localization observed in AD. Interestingly, N2a-APPswe cells displayed an increase in AKT activation and GSK3β inactivation, in the presence of Iso for 30 min (compared to untreated cells), suggesting that Iso might also induce Nrf2 activation through the PI3K-AKT-GSK3β pathway. Interestingly, according to a High Throughput Screening study performed by the team, Iso was also shown to modulate genes related not only with oxidative stress and inflammation, but also with glucose and iron metabolism (both defective in AD), in AD neuronal and neuroinflammation cell models, and in APP/PS1 mice at an early AD

stage (6 mo) unpublished data), which might be related to Iso-induced activation of PI3K-AKT-GSK3β pathway. Next, we also evaluated the expression of *Nrf2*-dependent genes. Interestingly, the results demonstrated that *Hmox1* (which was reduced in N2a-APPswe cells, compared to N2a-wt) and HMOX1 protein levels were significantly increased in diseased cells treated with Iso for 6 h (N2a-APPswe, compared to untreated cells). Moreover, other Nrf2-dependent genes, namely NAD(P) H quinone oxidoreductase 1 gene (*Nqo1*) and Superoxide dismutase 1 gene (*Sod1*), were also increased by Iso (Supplementary Fig. S2), corroborating Iso-induced Nrf2 activation. Importantly, both Nrf2 activation and increase in HMOX1 protein levels triggered by Iso in neurons suggest its potential role in neuroprotection. In fact, HMOX1 is associated with neurotoxicity, inflammation and accumulation of Aβ peptides (characteristic of AD), through a non-Nrf2-dependent pathway, in contrast to the neuroprotective effect of concomitant Nrf2 activation and HMOX1 expression, as reported in several cellular and animal models of neurodegenerative diseases (Nitti, 2018; Schipper et al, 2019; Sung et al, 2016).

Iso also demonstrated anti-inflammatory potential in LPS-stimulated microglia, where a decrease in the pro-inflammatory genes *Nos2* and *Il-1β* and in their encoded proteins, iNOS and pro-IL-1β respectively, and a reduction in NO production was observed.

Since our in chemico results suggested that Iso was able to cross the BBB and inhibit BACE1 activity, the potential therapeutic effect of Iso in AD was investigates in an AD mice model (APP/PS1). These animals display a predisposition to produce insoluble forms of Aβ, with astrocytosis and severe gliosis in the proximity of the developing plaques, at 6 months (Kamphuis et al, 2012) and formation of abundant plaques in the hippocampus and cortex, at 9 months of age (Jankowsky et al, 2004). We first administered 5 mo (that mimics AD early stage) APP/PS1 and WT female mice (with the same genetic background), with Iso (50 mg/kg), intranasally, for one month. Subsequently, Iso effect on some AD neuropathological hallmarks and cognitive function were evaluated. To ensure animal's well-being, the weight was weekly monitored and fasting glucose and triglycerides levels were determined on the day of sacrifice, in all the three study groups (WT, APP/PS1 and APP/PS1+Iso) of 6 mo mice. Iso seems to have increased the body weight which was accompanied by a non-significant increase in gonadal adipose tissue. It should also be noted that the transgenic mice showed increased adipose tissue compared to the WT counterparts. Both these facts might be explained, respectively, by the young age of this set of female animals as well as by the strain genetic background itself. In fact, this was not observed in 11 mo male mice, when the phenotype of the disease is fully installed as inferred by the neurochemical and cognitive results. Indeed, at this age, both APP/PS1 and WT animals are still overweighted compared to their female littermates

(data not shown). Interestingly, Iso significantly reduced the body weight throughout treatment, compared to non-treated animals (WT and APP/PS1). Accordingly, the same trends were observed in epididymal adipose tissue weight. Nevertheless, Iso treatment did not compromise animal well–being since body loss was less than 15%. Concerning triglycerides levels, Iso demonstrated beneficial effects by significantly reducing those in APP/PS1 mice.

Moreover, no alterations were observed among the three study groups of 6 mo mice, concerning triglycerides and glucose levels, although all the animals (that have the same genetic background) showed elevated values of glucose (hyperglycemia), as also observed in 11 mo mice. AD is characterized by cerebral insulin resistance, and it is known that insulin plays a key role in the peripheral control of blood glucose levels, in lipid and protein metabolism and is important in modulating brain function as a growth factor essential for neurogenesis (Ferreira et al, 2011). Regardless of pathology, it is reported that the transgenic background strain C57B/6J exhibits a tendency for elevated glucose levels in relation to significantly lower insulin secretion. Fasting in these animals also leads to a catabolic state, which allows for exacerbated mobilization of liver glucose and glycogen reserves resulting in a compensatory hyperglycemia (Benedé-Ubieto et al, 2020; Macklin et al, 2017). However, the glucose tolerance test performed in 11 mo mice was not affected either by the disease or Iso treatment.

As expected, APPS/PS1 animals displayed increased levels of $A\beta_{40}$ and $A\beta_{42}$ peptides in the brain, compared to WT mice, which were reduced in Iso treated APP/PS1 mice. This is in accordance with the results observed in N2a-APPswe cells (that produced higher levels of both peptides than N2a-wt cells), where a significant decrease of $A\beta_{40}$ was induced by Iso treatment, although no alterations were detected in $A\beta_{42}$ peptide levels. Nevertheless, these results are in accordance with Iso–induced Nrf2–ARE signaling pathway activation, that is negatively correlated with the gene expression of *BACE1* and the production of $A\beta$ peptides (Bahn et al, 2019). Overall, our data strongly suggest a potential effect of Iso in circumventing $A\beta$ accumulation in the brain.

At 6 mo (early AD stage) APP/PS1 animals showed increased anxious behavior, compared to WT mice, which is expected since anxiety is a prodromic symptom of AD. Although Iso administration did not significantly reduce the latency time to enter in the central zone of the open field arena compared to untreated APP/PS1 animals, it reduced it to levels not significantly different from those observed with WT animals. In contrast, diseased animals showed enhanced "freezing" behavior when in an environment associated to an aversive stimulus, that was not observed in Iso–treated mice. However, this was only detected in the training day of the Fear Conditioning test, with no alterations registered in the second

(evaluation of contextual memory) or third (evaluation of associative memory) days. We hypothesize that the % of total freezing observed in APP/PS1 non-treated mice in the first day might be related to animal's distrustfulness (compared to WT animals). As expected, in 11 mo animals no differences were observed in the exploratory behavior in the open field test and elevated plus maze between APP/PS1 and WT animals, and the corresponding treated groups.

Since no relevant phenotypic changes were detected at 6 mo, we performed a more robust study in older animals (11 mo), intranasally administered with a higher dose of Iso (100 mg/kg), for one month. Hence, we studied the pharmacokinetic profile of Iso and determined demographic, biochemical and histological alterations, in WT animals with the same genetic background as APP/PS1 transgenic mice, administered with the vehicle or Iso.

According to the pharmacokinetic study, Iso was absorbed quickly and removed from the blood due to either a fast distribution into peripheral tissues or elimination, which agrees with the results achieved by other authors, after Iso intravenous and oral administration (Hong et al, 2013; Badger et al, 2002). Our results showed that Iso was present in the brain, plasma and lungs, the latter displaying greater exposure after Iso intranasal administration. Comparing our results to those obtained by Hong et al. (2013), it seems that the systemic exposure of Iso after intranasal and intravenous administration routes are identical (and superior to the oral route). However, since there are no available data on Iso brain and lung exposure after intravenous and oral administration, it is not possible to compare these parameters with its intranasal administration, obtained in our study. Nevertheless, histological analyses of lung cryosections from Iso-treated mice revealed lymphocytes infiltration and bronchiolar hyperplasia compared to the samples obtained from mice administered with vehicle (PBS). However, bronchiolar hyperplasia was also observed in animals treated with PBS (VEH), suggesting that these events might be due to the administration route (intranasal) rather than to the compound (Iso) itself. Also, the occurrence of hepatic steatosis in the control animals and in Isoeugenol-treated mice, suggests a pattern of histopathological alterations in the livers of these animals. In contrast, kidney alterations (cellular eosinophilia and tubular epithelial hypertrophy) were only observed in Iso-treated animals. Curiously, some of these histopathological changes were also reported for the drug dimethyl fumarate, approved for the treatment of multiple sclerosis, which also belongs to the class of skin allergens that behave like Michael acceptors (Gold et al, 2022). Additional in vivo studies with lower doses of Iso should be conducted to verify the maintenance of drug efficacy with potential mitigation of the related histopathological alterations.

No relevant differences in the demographic and biochemical values were detected between untreated WT and APP/PS1 males' (administered with VEH). However, both groups were equally affected by Iso, which induced a significant decrease in animals' weight, probably related to Iso-induced metabolic alterations as observed in this study (e.g., reduction in LDL cholesterol and triglycerides, in 11 mo females and males, respectively), and by others (e.g., reduction of glucose blood levels in diabetic neuropathic rats (Alharthy et al, 2023). Importantly, similar results (including biochemical and metabolic) were obtained between the aged-matched WT and APP/PS1 females (treated with VEH only), regardless the significant increase in the adipose tissue weight in APP/PS1 animals, compared to the WT (which was also observed at 6 mo females). Also, Aβ peptides levels were similar among the cortex, hippocampus and plasma of APP/PS1 males and females (data not shown). These results indicate that potential differences between WT and APP/PS1 transgenic mice are not gender-related. Thus, we assume that conclusions might be drawn from 6 mo females and 11 mo males' data comparison.

In an attempt to ensure the detection of significant differences regarding neuropathological alterations among WT and APP/PS1 untreated and treated mice, the cortex and the hippocampus were dissected and used for gene expression and Aβ peptides levels analysis. In fact, we tried to detect alterations in the protein levels of APP, BACE1, iNOS, Pro-IL-1β, HMOX1 and p44/42 ERK, in the all brain of the 6 mo females (Supplementary Figure S3). However, among the proteins analyzed, we only found differences in the levels of APP and of p44/42 (involved in cell survival mechanisms and in ROS-induced Nrf2 nuclear translocation (Meng et al, 2013)). As expected, APP levels were significantly increased while p44/42 protein was significantly reduced in APP/PS1 animals compared to WT. Iso treatment did not induce alterations in the APP protein but increased the levels of p44/42 (APP/PS1 (Iso)) compared to APP/PS1 untreated animals).

Therefore, we evaluated Iso effect on the expression of genes related with APP overexpression and processing (*hAPP*, *Bace1*), inflammation (*Il-1β* and *Prkcg*), energy metabolism (*Ppargc1α*), oxidative stress (*Hmox1*), microglia function (*Trem2* and *Iba1*) and neuroprotection (*Bdnf*). The expression of *hAPP* gene was significantly increased in the cortex and hippocampus of APP/PS1 mice (compared to WT) and was not altered by Iso. These results were expected and are in accordance with those regarding the APP protein levels in the brain of 6 mo mice (Supplementary Fig. S3). We did not find alterations in the expression of *Bace1* gene between WT and APP/PS1 mice, either in cortex or hippocampus. However, *Bace1* gene expression decreased in the hippocampus of Iso-treated WT animals (compared to untreated mice), and was (non-significantly) reduced (2.25-fold) in APP/PS1 mice administered with Iso (compared to

APP/PS1 untreated mice), in a similar pattern as observed for BACE1 protein levels in 6 mo mice brain (Supplementary Fig. S3). These results suggest that Iso might act mainly at the level of BACE1 enzymatic activity, as supported by its inhibition demonstrated by the in chemico analysis in our study, and the reduced levels of Aβ peptides induced by Iso, in vitro and in vivo. As expected, higher levels of both $A\beta_{40}$ and $A\beta_{42}$ peptides were detected in APP/PS1 mice cortex, hippocampus and also in plasma (compared to WT mice). Iso treatment decreased Aβ peptides levels in the plasma and in the cortex ($A\beta_{40}$ levels only), with no alterations observed in the hippocampus of APP/PS1 mice at a late AD stage. Since the hippocampus is the initial region of Aβ accumulation and neuronal damage (Murray et al, 2014), these results might be related to the overaccumulation of Aβ in aged-mice brain that could not be reverted by Iso in such an advanced state.

Moreover, *Ppargc1α* mRNA levels were significantly reduced in the hippocampus of untreated APP/PS1 mice (compared to WT) and increased in Iso-treated APP/PS1 animals. *Ppargc1α* encodes the PGC-1α protein, that is involved in lipid, glucose and energy metabolism and is reduced in human AD brain and AD mice models, including the APP/PS1 used in this study (Mota and Sastre, 2021). The increase in *Ppargc1α* gene expression might also contribute to the Aβ peptides levels reduction in AD mice treated with Iso, since PGC-1α overexpression was shown to diminish Aβ production, particularly by regulating the expression of BACE1 enzyme (reviewed in Mota and Sastre, 2021). Interestingly, Iso induced a reduction in *Prkcg* gene expression, in both the cortex and hippocampus of WT animals. *Prkcg* encodes the protein kinase C-gamma (PKCγ) protein that was shown to be increased in human AD brain and to correlate with increased BACE1 protein levels and BACE1-mediated APP cleavage and Aβ production (Du et al, 2018). The authors showed that APP/PS1 mice treated with the PKCγ-inhibitor rottlerin- displayed reduced BACE1 expression and APP processing. Moreover, these animals showed improved spatial learning and memory deficits (Du et al, 2018). In our study, despite that no differences were detected among WT and APP/PS1 mice, a non-significant decrease of 2.8 fold in the expression of *Prkcg* was detected in APP/PS1 treated animals. In line with Du and colleagues' work (2018), in this study Iso treatment reverted the memory impairment of aged APP/PS1 mice (at a late AD stage), as concluded from the Y-MAZE and Novel Object Recognition tests evaluating short-term spatial and recognition memory, respectively, and by the Fear Conditioning test, that evaluates hippocampal-dependent long-term contextual/associative memory.

We did not find significant differences in *Il-1β* gene expression, between WT and APP/PS1 mice, either in the cortex or hippocampus. Apart from a significant decrease in Iso-induced *Il-1β* mRNA levels observed

in the hippocampus of WT animals (compared to untreated WT mice), no other alterations were detected. These results agree with the pro–IL–1β protein levels determined in 6 mo animals (Supplementary Fig. S3) and with observations made by others (Franco–Bocanegra et al, 2019), where no alterations in the levels of IL–1β were detected, in a *post-mortem* AD study.

Despite the lack of differences in *Iba1* expression between WT and APP/PS1 mice, it was significantly induced in transgenic animals treated with Iso. Iba1 is essential for microglial migration and phagocytosis and microglia motility has been demonstrated to be altered in AD (Krabbe et al, 2013). These results are in accordance with the work of Franco–Bocanegra and colleagues (2019), that also did not observe significant differences between AD and the control group but detected an increase in Iba1, in the brain of AD patients submitted to Aβ immunotherapy. Furthermore, the authors suggested that this increase might reflect microglia motility changes associated with phagocytosis, and showed that Aβ immunotherapy-induced Iba1 increase was associated with a less pro-inflammatory environment than observed in AD (Franco–Bocanegra et al, 2019). Additionally, *Trem2* gene expression was significantly increased in the cortex and was slightly augmented in the hippocampus of diseased animals (APP/PS1, compared to WT). *Trem2* encodes TREM2 immune receptor, which is mainly expressed on microglia and is implicated in complex signaling pathways related to inflammatory signaling, microglial metabolism and function, and lipid homeostasis (reviewed in Li et al, 2022). Recently, Keren–Shaul and colleagues (2017) identified a novel and unique microglia phenotype associated to AD, using the 5XFAD AD mouse model. The authors showed that under stressful conditions, microglia shift to a disease-associated microglia (DAM) profile and functional TREM2 receptor is required for this transition (Keren–Shaul et al, 2017). In fact, TREM2 variants were demonstrated to be related to AD pathogenesis (Colonna and Wang, 2016). DAM profile pretends to be neuroprotective since DAM was found near to Aβ plaques and was positively stained for intracellular Aβ particles (in both 5XFAD mice and in human AD postmortem brains) (Keren–Shaul et al, 2017). More recently, the overexpression of TREM2 in the brain of APP/PS1 transgenic mice, was shown to rescue diseased-animals' spatial cognitive deficits, decreased Aβ plaques burden and ameliorated inflammation (Ruganzu et al, 2021). Considering the aforementioned, the increase in *Trem2* expression that we observed in the cortex of APP/PS1 animals might be related to an increase in DAM. Despite there were no significant differences in *Trem2* gene among Iso-treated and untreated APP/PS1 mice, Iso induced a slight but consistent increase in its expression (by 1.5 fold in both the cortex and the hippocampus), and significantly reduced *Trem2* expression in the hippocampus of WT mice. These results together with the significant increase in *Iba1* in APP/PS1 mice administered with Iso,

strongly suggests that Iso might enhance microglia function towards neuroprotection in AD. In fact, *Bdnf* gene expression was also increased by Iso, in the hippocampus of AD mice. *Bdnf* encodes the Brain-derived neurotrophic factor (BDNF), which is crucial for neuronal support. BDNF levels were shown to be reduced in the serum and brain of AD patients and in a mouse model of tauopathy (Jiao et al, 2016) and BDNF administration ameliorated the learning deficits in an AD rat model (Zhang et al, 2015). Interestingly, BDNF is also involved in ROS-induced Nrf2 nuclear translocation, which requires ERK1/2 activation, as observed in primary hippocampal neurons (Bruna et al, 2018).

A significant increase in *Hmox1* gene expression was also observed, in both WT and APP/PS1 treated mice (compared to their respective untreated group), which is in accordance with Iso-induced Nrf2 activation, supporting its antioxidant effect both in vitro and in vivo.

5. Conclusions

The most successful Nrf2 activator is dimethyl fumarate (Tecfidera, Biogen Inc.), which was initially approved for the treatment of psoriasis and further developed for remitting relapsing multiple sclerosis. Since its approval for this pathology in 2013, it has remained the only marketed drug that claims to target Nrf2, albeit not specifically. The most successful case to date in the context of neurodegenerative diseases is omaveloxone (Reata Pharmaceuticals), a difluoromethyl acetamide derivative of bardoxolone that received FDA approval as the first and only drug indicated for patients with Friedreich ataxia. The study herein presented is the first to demonstrate the beneficial effects of the Nrf2 activating molecule Isoeugenol in a preclinical model of Alzheimer´s disease, improving the outcome of the main disease-associated hallmarks. The fact that Isoeugenol decreased the levels of Aβ peptides, restrained oxidative stress and neuroinflammation and improved the memory deficits observed in APP/PS1 mice, positions Isoeugenol as a promising therapeutic strategy for AD, bringing great hope for the implementation of this new therapeutic approach for this devastating disease that attack the essence of our humanity.

Statements and Declarations

CRediT author statement

Ana Silva: Investigation, Writing - Original draft preparation and Reviewing and Editing; **Jéssica Macedo:** Investigation, Writing - Original draft preparation; **Patrícia Moreira:** Investigation, Writing - Original draft preparation; **Sónia Silva:** Investigation; Writing - Original draft preparation; **Joana Bicker:**

Investigation, Writing - Original draft preparation; **Ana Fortuna:** Methodology; Validation; Reviewing and Editing; **Joana Liberal:** Investigation; **Beatriz Rodrigues:** Investigation; **Rosa Resende:** Investigation; **Armanda E. Santos:** Resources; Reviewing and Editing; **Cláudia Pereira:** Funding acquisition; Reviewing and Editing; **Maria Teresa Cruz:** Conceptualization; Funding acquisition; Supervision; Project administration; Resources; Reviewing and Editing.

Declaration of competing interest

The authors declare no conflict of interest

References

- Alharthy KM, Balaha MF, Devi S, Altharawi A, Yusufoglu HS, Aldossari RM, Alam A, Giacomo VD. Ameliorative Effects of Isoeugenol and Eugenol against Impaired Nerve Function and Inflammatory and Oxidative Mediators in Diabetic Neuropathic Rats. Biomedicines 2023;11(4):1203. doi: 10.3390/biomedicines11041203.

- Ali T, Kim T, Rehman SU, Khan MS, Amin FU, Khan M, Ikram M, Kim MO. Natural Dietary Supplementation of Anthocyanins via PI3K/Akt/Nrf2/HO-1 Pathways Mitigate Oxidative Stress, Neurodegeneration, and Memory Impairment in a Mouse Model of Alzheimer's Disease. Mol Neurobiol. 2018 Jul;55(7):6076-6093. doi: 10.1007/s12035-017-0798-6.

- Ambacher KK, Pitzul KB, Karajgikar M, Hamilton A, Ferguson SS, Cregan SP. The JNK- and AKT/GSK3β- signaling pathways converge to regulate Puma induction and neuronal apoptosis induced by trophic factor deprivation. PLoS One. 2012;7(10):e46885. doi: 10.1371/journal.pone.0046885.

- Atsumi T, Fujisawa S, Tonosaki K. A comparative study of the antioxidant/prooxidant activities of eugenol and isoeugenol with various concentrations and oxidation conditions. Toxicol In Vitro. 2005 Dec;19(8):1025-33. doi: 10.1016/j.tiv.2005.04.012.

- Badger DA, Smith RL, Bao J, Kuester RK, Sipes IG. Disposition and metabolism of isoeugenol in the male Fischer 344 rat. Food Chem Toxicol. 2002;40(12):1757-1765. doi:10.1016/S0278-6915(02)00183-7.

- Bahn G, Jo DG. Therapeutic Approaches to Alzheimer's Disease Through Modulation of NRF2. Neuromolecular Med 2019;21(1):1-11. doi: 10.1007/s12017-018-08523-5.

- Bahn G, Park JS, Yun UJ, Lee YJ, Choi Y, Park JS, Baek SH, Choi BY, Cho YS, Kim HK, Han J, Sul JH, Baik SH, Lim J, Wakabayashi N, Bae SH, Han JW, Arumugam TV, Mattson MP, Jo DG. NRF2/ARE pathway negatively regulates BACE1 expression and ameliorates cognitive deficits in mouse Alzheimer's models. Proc Natl Acad Sci U S A. 2019 Jun 18;116(25):12516-12523. doi: 10.1073/pnas.1819541116.

- Battino M, Giampieri F, Pistollato F, Sureda A, de Oliveira MR, Pittalà V, Fallarino F, Nabavi SF, Atanasov AG, Nabavi SM. Nrf2 as regulator of innate immunity: A molecular Swiss army knife! Biotechnol Adv. 2018 Mar-Apr;36(2):358-370. doi: 10.1016/j.biotechadv.2017.12.012.

- Bellezza I, Giambanco I, Minelli A, Donato R. Nrf2-Keap1 signaling in oxidative and reductive stress. Biochim Biophys Acta Mol Cell Res. 2018 May;1865(5):721-733. doi: 10.1016/j.bbamcr.2018.02.010.

- Benedé-Ubieto R, Estévez-Vázquez O, Ramadori P, Cubero FJ, Nevzorova YA. Guidelines and Considerations for Metabolic Tolerance Tests in Mice. Diabetes Metab Syndr Obes. 2020 Feb 18;13:439-450. doi: 10.2147/DMSO.S234665.

- Bicker J, Alves G, Fortuna A, Soares-da-Silva P, Falcão A. A new PAMPA model using an in-house brain lipid extract for screening the blood-brain barrier permeability of drug candidates. Int J Pharm. 2016 Mar 30;501(1-2):102-11. doi: 10.1016/j.ijpharm.2016.01.074.

- Boulebd H. DFT study of the antiradical properties of some aromatic compounds derived from antioxidant essential oils: C-H bond vs. O-H bond. Free Radic Res. 2019 Dec;53(11-12):1125-1134. doi: 10.1080/10715762.2019.1690652.

- Breijyeh Z, Karaman R. Comprehensive Review on Alzheimer's Disease: Causes and Treatment. Molecules. 2020 Dec 8;25(24):5789. doi: 10.3390/molecules25245789.

- Bruna B, Lobos P, Herrera-Molina R, Hidalgo C, Paula-Lima A, Adasme T. The signaling pathways underlying BDNF-induced Nrf2 hippocampal nuclear translocation involve ROS, RyR-Mediated Ca2+ signals, ERK and PI3K. Biochem Biophys Res Commun. 2018 Oct 20;505(1):201-207. doi: 10.1016/j.bbrc.2018.09.080.

- Calsolaro V, Edison P. Neuroinflammation in Alzheimer's disease: Current evidence and future directions. Alzheimers Dement. 2016 Jun;12(6):719-32. doi: 10.1016/j.jalz.2016.02.010..

- Cheignon C, Tomas M, Bonnefont-Rousselot D, Faller P, Hureau C, Collin F. Oxidative stress and the amyloid beta peptide in Alzheimer's disease. Redox Biol. 2018 Apr;14:450-464. doi: 10.1016/j.redox.2017.10.014.

- Chen WW, Zhang X, Huang WJ. Role of neuroinflammation in neurodegenerative diseases (Review). Mol Med Rep. 2016 Apr;13(4):3391-6. doi: 10.3892/mmr.2016.4948.

- Coimbra JRM, Baptista SJ, Dinis TCP, Silva MMC, Moreira PI, Santos AE, Salvador JAR. Combining Virtual Screening Protocol and In Vitro Evaluation towards the Discovery of BACE1 Inhibitors. Biomolecules. 2020 Apr 1;10(4):535. doi: 10.3390/biom10040535.

- Colonna M, Wang Y. TREM2 variants: new keys to decipher Alzheimer disease pathogenesis. Nat Rev Neurosci. 2016 Apr;17(4):201-7. doi: 10.1038/nrn.2016.7.

- Cuadrado, A. NRF2 in neurodegenerative diseases. Curr Opin Toxicol. 2016;2:46–53. doi: 10.1016/j.cotox.2016.09.004.

- Cuadrado A, Kügler S, Lastres-Becker I. Pharmacological targeting of GSK-3 and NRF2 provides neuroprotection in a preclinical model of tauopathy. Redox Biol. 2018 Apr;14:522-534. doi: 10.1016/j.redox.2017.10.010.

- Cuadrado A. Brain-Protective Mechanisms of Transcription Factor NRF2: Toward a Common Strategy for Neurodegenerative Diseases. Annu Rev Pharmacol Toxicol. 2022 Jan 6;62:255-277. doi: 10.1146/annurev-pharmtox-052220-103416

- Dong Y, Li X, Cheng J, Hou L. Drug Development for Alzheimer's Disease: Microglia Induced Neuroinflammation as a Target? Int J Mol Sci. 2019 Jan 28;20(3):558. doi: 10.3390/ijms20030558.

- Du Y, Zhao Y, Li C, Zheng Q, Tian J, Li Z, Huang TY, Zhang W, Xu H. Inhibition of PKCδ reduces amyloid-β levels and reverses Alzheimer disease phenotypes. J Exp Med. 2018 Jun 4;215(6):1665-1677. doi: 10.1084/jem.20171193.

- EMA - European Medicines Agency. Tecfidera: EPAR - Product Information (PDF/705.73 KB). (Last updated: 20/09/2023) URL: https://www.ema.europa.eu/en/medicines/human/EPAR/tecfidera (accessed 22/11/2023).

- Fão L, Mota SI, Rego AC. Shaping the Nrf2-ARE-related pathways in Alzheimer's and Parkinson's diseases. Ageing Res Rev. 2019 Sep;54:100942. doi: 10.1016/j.arr.2019.100942.

- Ferreira, L. T., Saviolli, I. H., Valenti, V. E. & Abreu, L. C. de. Diabetes melito: hiperglicemia crônica e suas complicações. Arquivos Brasileiros de Ciências da Saúde 2011;36:182–188. doi: 10.7322/abcs.v36i3.59

- Fındık E, Ceylan M, Elmastaş M. Isoeugenol-based novel potent antioxidants: synthesis and reactivity. Eur J Med Chem. 2011 Sep;46(9):4618-24. doi: 10.1016/j.ejmech.2011.07.041.

- Fortuna A, Alves G, Serralheiro A, Sousa J, Falcão A. Intranasal delivery of systemic-acting drugs: small-molecules and biomacromolecules. Eur J Pharm Biopharm. 2014;88(1):8-27. doi:10.1016/j.ejpb.2014.03.004.

- Franco-Bocanegra DK, George B, Lau LC, Holmes C, Nicoll JAR, Boche D. Microglial motility in Alzheimer′s disease and after Aβ42 immunotherapy: a human post-mortem study. Acta Neuropathol Commun. 2019 Nov 8;7(1):174. doi: 10.1186/s40478-019-0828-x.

- Gabbouj S, Ryhänen S, Marttinen M, Wittrahm R, Takalo M, Kemppainen S, Martiskainen H, Tanila H, Haapasalo A, Hiltunen M, Natunen T. Altered Insulin Signaling in Alzheimer′s Disease Brain - Special Emphasis on PI3K-Akt Pathway. Front Neurosci. 2019 Jun 18;13:629. doi: 10.3389/fnins.2019.00629.

- Alzheimer′s Association. 2016 Alzheimer′s disease facts and figures. Alzheimer's Dement. 2016 Apr;12(4):459-509. doi: 10.1016/j.jalz.2016.03.001.

- Alzheimer′s Association. 2020 Alzheimer′s disease facts and figures. Alzheimer′s Dement. 2020;16:391-460. doi: 10.1002/alz.12068

- Geerts H, Grossberg GT. Pharmacology of acetylcholinesterase inhibitors and N-methyl-D-aspartate receptors for combination therapy in the treatment of Alzheimer′s disease. J Clin Pharmacol. 2006 Jul;46(7 Suppl 1):8S-16S. doi: 10.1177/0091270006288734.

- Gold R, Arnold DL, Bar-Or A, Fox RJ, Kappos L, Mokliatchouk O, Jiang X, Lyons J, Kapadia S, Miller C. Long-term safety and efficacy of dimethyl fumarate for up to 13 ears in patients with relapsing-remitting multiple sclerosis: Final ENDORSE study results. Mult Scler. 2022 Apr;28(5):801-816. doi: 10.1177/13524585211037909.

- Gonçalves J, Bicker J, Gouveia F, Liberal J, Oliveira RC, Alves G, Falcão A, Fortuna A. Nose-to-brain delivery of levetiracetam after intranasal administration to mice. Int J Pharm. 2019 Jun 10;564:329-339. doi: 10.1016/j.ijpharm.2019.04.047.

- Gonçalves J, Alves G, Fonseca C, Carona A, Bicker J, Falcão A, Fortuna A. Is intranasal administration an opportunity for direct brain delivery of lacosamide? Eur J Pharm Sci. 2021 Feb 1;157:105632. doi: 10.1016/j.ejps.2020.105632.

- Green LC, Wagner DA, Glogowski J, Skipper PL, Wishnok JS, Tannenbaum SR. Analysis of nitrate, nitrite, and [15N] nitrate in biological fluids. Anal Biochem. 1982 Oct;126(1):131-8. doi: 10.1016/0003-2697(82)90118-x.

- Hanson, L. R., Fine, J. M., Svitak, A. L. & Faltesek, K. A. Intranasal administration of CNS therapeutics to awake mice. Journal of visualized experiments: JoVE 1–7 (2013) doi:10.3791/4440.

- Heron M. Deaths: leading causes for 2004. Natl Vital Stat Rep 2007;56(5):1-95. PMID: 18092547.

- Hong SP, Fuciarelli AF, Johnson JD, et al. Toxicokinetics of Isoeugenol in F344 rats and B6C3F1 mice. Xenobiotica. 2013;43(11):1010-1017. doi:10.3109/00498254.2013.790576

- ICH - International Council for Harmonisation of Technical Requirements for Pharmaceuticals for Human Use. Guideline M10 on Bioanalytical Method Validation. 2019 Mar;1-60.

- Jankowsky JL, Fadale DJ, Anderson J, Xu GM, Gonzales V, Jenkins NA, Copeland NG, Lee MK, Younkin LH, Wagner SL, Younkin SG, Borchelt DR. Mutant presenilins specifically elevate the levels of the 42 residue beta-amyloid peptide in vivo: evidence for augmentation of a 42-specific gamma secretase. Hum Mol Genet. 2004 Jan 15;13(2):159-70. doi: 10.1093/hmg/ddh019.

- Jiao SS, Shen LL, Zhu C, Bu XL, Liu YH, Liu CH, Yao XQ, Zhang LL, Zhou HD, Walker DG, Tan J, Götz J, Zhou XF, Wang YJ. Brain-derived neurotrophic factor protects against tau-related neurodegeneration of Alzheimer's disease. Transl Psychiatry. 2016 Oct 4;6(10):e907. doi: 10.1038/tp.2016.186.

- Kamphuis W, Mamber C, Moeton M, Kooijman L, Sluijs JA, Jansen AH, Verveer M, de Groot LR, Smith VD, Rangarajan S, Rodríguez JJ, Orre M, Hol EM. GFAP isoforms in adult mouse brain with a focus on neurogenic astrocytes and reactive astrogliosis in mouse models of Alzheimer disease. PLoS One. 2012;7(8):e42823. doi: 10.1371/journal.pone.0042823.

- Kaundal RK, Datusalia AK, Sharma SS. Posttranscriptional regulation of Nrf2 through miRNAs and their role in Alzheimer's disease. Pharmacol Res. 2022 Jan;175:106018. doi: 10.1016/j.phrs.2021.106018.

- Keren-Shaul H, Spinrad A, Weiner A, Matcovitch-Natan O, Dvir-Szternfeld R, Ulland TK, David E, Baruch K, Lara-Astaiso D, Toth B, Itzkovitz S, Colonna M, Schwartz M, Amit I. A Unique Microglia Type Associated with Restricting Development of Alzheimer's Disease. Cell. 2017 Jun 15;169(7):1276-1290.e17. doi: 10.1016/j.cell.2017.05.018.

- Krabbe G, Halle A, Matyash V, Rinnenthal JL, Eom GD, Bernhardt U, Miller KR, Prokop S, Kettenmann H, Heppner FL. Functional impairment of microglia coincides with Beta-amyloid deposition in mice with Alzheimer-like pathology. PLoS One. 2013;8(4):e60921. doi: 10.1371/journal.pone.0060921.

- Lane CA, Hardy J, Schott JM. Alzheimer's disease. Eur J Neurol. 2018 Jan;25(1):59-70. doi: 10.1111/ene.13439.

- Li W, Tsubouchi R, Qiao S, Haneda M, Murakami K, Yoshino M. Inhibitory action of eugenol compounds on the production of nitric oxide in RAW264.7 macrophages. Biomed Res. 2006 Apr;27(2):69-74. doi: 10.2220/biomedres.27.69.

- Li RY, Qin Q, Yang HC, Wang YY, Mi YX, Yin YS, Wang M, Yu CJ, Tang Y. TREM2 in the pathogenesis of AD: a lipid metabolism regulator and potential metabolic therapeutic target. Mol Neurodegener. 2022 Jun 3;17(1):40. doi: 10.1186/s13024-022-00542-y.

- Macklin L, Griffith CM, Cai Y, Rose GM, Yan XX, Patrylo PR. Glucose tolerance and insulin sensitivity are impaired in APP/PS1 transgenic mice prior to amyloid plaque pathogenesis and cognitive decline. Exp Gerontol. 2017 Feb;88:9-18. doi: 10.1016/j.exger.2016.12.019.

- Majkutewicz I, Kurowska E, Podlacha M, Myślińska D, Grembecka B, Ruciński J, Plucińska K, Jerzemowska G, Wrona D. Dimethyl fumarate attenuates intracerebroventricular streptozotocin-induced spatial memory impairment and hippocampal neurodegeneration in rats. Behav Brain Res. 2016 Jul 15;308:24-37. doi: 10.1016/j.bbr.2016.04.012.

- Masters CL, Bateman R, Blennow K, Rowe CC, Sperling RA, Cummings JL. Alzheimer's disease. Nat Rev Dis Primers. 2015 Oct 15;1:15056. doi: 10.1038/nrdp.2015.56.

- Meng XB, Sun GB, Wang M, Sun J, Qin M, Sun XB. P90RSK and Nrf2 Activation via MEK1/2-ERK1/2 Pathways Mediated by Notoginsenoside R2 to Prevent 6-Hydroxydopamine-Induced Apoptotic Death in SH-SY5Y Cells. Evid Based Complement Alternat Med. 2013;2013:971712. doi: 10.1155/2013/971712.

- Mota SI, Costa RO, Ferreira IL, Santana I, Caldeira GL, Padovano C, Fonseca AC, Baldeiras I, Cunha C, Letra L, Oliveira CR, Pereira CM, Rego AC. Oxidative stress involving changes in Nrf2 and ER stress in early stages of Alzheimer's disease. Biochim Biophys Acta. 2015 Jul;1852(7):1428-41. doi: 10.1016/j.bbadis.2015.03.015.

- Mota BC, Sastre M. The Role of PGC1α in Alzheimer's Disease and Therapeutic Interventions. Int J Mol Sci. 2021 May 28;22(11):5769. doi: 10.3390/ijms22115769.

- Murray ME, Przybelski SA, Lesnick TG, Liesinger AM, Spychalla A, Zhang B, Gunter JL, Parisi JE, Boeve BF, Knopman DS, Petersen RC, Jack CR Jr, Dickson DW, Kantarci K. Early Alzheimer's disease neuropathology detected by proton MR spectroscopy. J Neurosci. 2014 Dec 3;34(49):16247-55. doi: 10.1523/JNEUROSCI.2027-14.2014.

- Natsch A. The Nrf2-Keap1-ARE toxicity pathway as a cellular sensor for skin sensitizers--functional relevance and a hypothesis on innate reactions to skin sensitizers. Toxicol Sci. 2010 Feb;113(2):284-92. doi: 10.1093/toxsci/kfp228.

- Natsch A, Ryan CA, Foertsch L, Emter R, Jaworska J, Gerberick F, Kern P. A dataset on 145 chemicals tested in alternative assays for skin sensitization undergoing prevalidation. J Appl Toxicol. 2013 Nov;33(11):1337-52. doi: 10.1002/jat.2868.

- Nitti M, Piras S, Brondolo L, Marinari UM, Pronzato MA, Furfaro AL. Heme Oxygenase 1 in the Nervous System: Does It Favor Neuronal Cell Survival or Induce Neurodegeneration? Int J Mol Sci. 2018 Aug 1;19(8):2260. doi: 10.3390/ijms19082260.

- Prasad SN, Muralidhara. Neuroprotective efficacy of eugenol and isoeugenol in acrylamide-induced neuropathy in rats: behavioral and biochemical evidence. Neurochem Res. 2013 Feb;38(2):330-45. doi: 10.1007/s11064-012-0924-9.

- Ramsey CP, Glass CA, Montgomery MB, Lindl KA, Ritson GP, Chia LA, Hamilton RL, Chu CT, Jordan-Sciutto KL. Expression of Nrf2 in neurodegenerative diseases. J Neuropathol Exp Neurol. 2007 Jan;66(1):75-85. doi: 10.1097/nen.0b013e31802d6da9.

- Rauscher FM, Sanders RA, Watkins JB 3rd. Effects of isoeugenol on oxidative stress pathways in normal and streptozotocin-induced diabetic rats. J Biochem Mol Toxicol. 2001;15(3):159-64. doi: 10.1002/jbt.13.

- Robledinos-Antón N, Fernández-Ginés R, Manda G, Cuadrado A. Activators and Inhibitors of NRF2: A Review of Their Potential for Clinical Development. Oxid Med Cell Longev. 2019 Jul 14;2019:9372182. doi: 10.1155/2019/9372182.

- Ruehl-Fehlert C, Kittel B, Morawietz G, Deslex P, Keenan C, Mahrt CR, Nolte T, Robinson M, Stuart BP, Deschl U, RITA Group, NACAD Group. Revised guides for organ sampling and trimming in rats and mice--part 1. Exp Toxicol Pathol. 2003 Sep;55(2-3):91-106. doi: 10.1078/0940-2993-00311.

- Ruganzu JB, Zheng Q, Wu X, He Y, Peng X, Jin H, Zhou J, Ma R, Ji S, Ma Y, Qian Y, Wang Y, Yang W. TREM2 overexpression rescues cognitive deficits in APP/PS1 transgenic mice by reducing neuroinflammation via the JAK/STAT/SOCS signaling pathway. Exp Neurol. 2021 Feb;336:113506. doi: 10.1016/j.expneurol.2020.113506.

- Schipper HM, Song W, Tavitian A, Cressatti M. The sinister face of heme oxygenase-1 in brain aging and disease. Prog Neurobiol. 2019 Jan;172:40-70. doi: 10.1016/j.pneurobio.2018.06.008.

- Schneider LS. Alzheimer disease pharmacologic treatment and treatment research. Continuum (Minneap Minn). 2013 Apr;19(2 Dementia):339-57. doi: 10.1212/01.CON.0000429180.60095.d0.

- Serralheiro A, Alves G, Fortuna A, Falcão A. Direct nose-to-brain delivery of lamotrigine following intranasal administration to mice. Int J Pharm. 2015;490(1-2):39-46. doi:10.1016/j.ijpharm.2015.05.021.

- Serrano-Pozo A, Frosch MP, Masliah E, Hyman BT. Neuropathological alterations in Alzheimer disease. Cold Spring Harb Perspect Med. 2011 Sep;1(1):a006189. doi: 10.1101/cshperspect.a006189.

- Silva A, Pereira M, Carrascal MA, Brites G, Neves B, Moreira P, Resende R, Silva MM, Santos AE, Pereira C, Cruz MT. Calcium Modulation, Anti-Oxidant and Anti-Inflammatory Effect of Skin Allergens

Targeting the Nrf2 Signaling Pathway in Alzheimer's Disease Cellular Models. Int J Mol Sci. 2020 Oct 21;21(20):7791. doi: 10.3390/ijms21207791.

- Silva S, Bicker J, Fonseca C, Ferreira NR, Vitorino C, Alves G, Falcão A, Fortuna A. Encapsulated Escitalopram and Paroxetine Intranasal Co-Administration: In Vitro/In Vivo Evaluation. Front Pharmacol. 2021 Dec 2;12:751321. doi: 10.3389/fphar.2021.751321.

- Song C, Shi J, Zhang P, Zhang Y, Xu J, Zhao L, Zhang R, Wang H, Chen H. Immunotherapy for Alzheimer's disease: targeting β-amyloid and beyond. Transl Neurodegener. 2022 Mar 18;11(1):18. doi: 10.1186/s40035-022-00292-3.

- Sung HY, Choi BO, Jeong JH, Kong KA, Hwang J, Ahn JH. Amyloid Beta-Mediated Hypomethylation of Heme Oxygenase 1 Correlates with Cognitive Impairment in Alzheimer's Disease. PLoS One. 2016 Apr 8;11(4):e0153156. doi: 10.1371/journal.pone.0153156.

- Takeyoshi M, Iida K, Suzuki K, Yamazaki S. Skin sensitization potency of isoeugenol and its dimers evaluated by a non-radioisotopic modification of the local lymph node assay and guinea pig maximization test. J Appl Toxicol. 2008 May;28(4):530-4. doi: 10.1002/jat.1305.

- Tarawneh R, Holtzman DM. The clinical problem of symptomatic Alzheimer disease and mild cognitive impairment. Cold Spring Harb Perspect Med. 2012 May;2(5):a006148. doi: 10.1101/cshperspect.a006148.

- Taylor JP, Hardy J, Fischbeck KH. Toxic proteins in neurodegenerative disease. Science. 2002 Jun 14;296(5575):1991-5. doi: 10.1126/science.1067122.

- Tönnies E, Trushina E. Oxidative Stress, Synaptic Dysfunction, and Alzheimer's Disease. J Alzheimers Dis. 2017;57(4):1105-1121. doi: 10.3233/JAD-161088.

- Van Eldik LJ, Carrillo MC, Cole PE, Feuerbach D, Greenberg BD, Hendrix JA, Kennedy M, Kozauer N, Margolin RA, Molinuevo JL, Mueller R, Ransohoff RM, Wilcock DM, Bain L, Bales K. The roles of inflammation and immune mechanisms in Alzheimer's disease. Alzheimers Dement (N Y). 2016 May 30;2(2):99-109. doi: 10.1016/j.trci.2016.05.001.

- Wang X, Zhou X, Li G, Zhang Y, Wu Y, Song W. Modifications and Trafficking of APP in the Pathogenesis of Alzheimer's Disease. Front Mol Neurosci. 2017 Sep 15;10:294. doi: 10.3389/fnmol.2017.00294.

- Wang R, Hu X, Pan J, Zhang G, Gong D. Interaction of Isoeugenol with calf thymus DNA and its protective effect on DNA oxidative damage. J Mol Liq. 2019;282:356–365. doi: 10.1016/j.molliq.2019.03.018

- WHO - World Health Organization. DEMENTIA: A public health priority (24/8/2012). 2012 URL: https://www.who.int/publications/i/item/dementia-a-public-health-priority.

- WHO - World Health Organization. Global action plan on the public health response to dementia 2017 – 2025. (7/12/2017). 2017 URL: https://www.who.int/publications/i/item/global-action-plan-on-the-public-health-response-to-dementia-2017---2025

- Zhang BY, Saijilafu, Liu CM, Wang RY, Zhu Q, Jiao Z, Zhou FQ. Akt-independent GSK3 inactivation downstream of PI3K signaling regulates mammalian axon regeneration. Biochem Biophys Res Commun. 2014 Jan 10;443(2):743-8. doi: 10.1016/j.bbrc.2013.12.037.

- Zhang L, Fang Y, Lian Y, Chen Y, Wu T, Zheng Y, Zong H, Sun L, Zhang R, Wang Z, Xu Y. Brain-derived neurotrophic factor ameliorates learning deficits in a rat model of Alzheimer's disease induced by aβ1-42. PLoS One. 2015 Apr 7;10(4):e0122415. doi: 10.1371/journal.pone.0122415.

- Zuroff L, Daley D, Black KL, Koronyo-Hamaoui M. Clearance of cerebral Aβ in Alzheimer's disease: reassessing the role of microglia and monocytes. Cell Mol Life Sci. 2017 Jun;74(12):2167-2201. doi: 10.1007/s00018-017-2463-7.

Supplementary data: available at https://doi.org/10.32388/LUXM7W

Declarations

Potential competing interests: No potential competing interests to declare.